Generalized statistical dynamical theory of x-ray diffraction by imperfect multilayer crystal structures with defects

S. I. Olikhovskii,[1,*] V. B. Molodkin,[1,2] E. G. Len,[1,2] E. S. Skakunova,[1] and S. V. Lizunova[1]
[1]*G. V. Kurdyumov Institute for Metal Physics, NAS of Ukraine, 36 Academician Vernadsky Boulevard, UA-03142 Kyiv, Ukraine*
[2]*Kyiv Academic University, NAS and MES of Ukraine, 36 Academician Vernadsky Boulevard, UA-03142 Kyiv, Ukraine*

(Received 11 February 2019; revised manuscript received 23 May 2019; published 18 June 2019)

The generalized statistical dynamical theory of x-ray scattering by imperfect single crystals with randomly distributed Coulomb-type defects has been extended to characterize structure imperfections in the real multilayers of arbitrary thickness in Bragg diffraction geometry. The recurrence relations for the coherent amplitude reflection and transmission coefficients of such multilayers, which consist of any number of layers with constant strain and randomly distributed defects in each one, have been derived within the concept of the dynamical wave field, i.e., the so-called Ewald-Bethe-Laue approach, with rigorous accounting for boundary conditions at layer interfaces. The analytical expression for the differential dynamical diffuse component of the reflection coefficient of an imperfect multilayer system has been obtained as well. This expression establishes direct connection between the distribution of the diffuse scattering intensity in a momentum space and statistical characteristics of defects in each layer. In addition, the integrals from differential diffuse scattering intensity over the Ewald sphere and over vertical divergence have been found, which correspond to diffuse components in measurements of rocking curves and reciprocal space maps, respectively. The developed theory provides the dynamical description for the one- and two-dimensional angular distributions of the mutually consistent coherent and diffuse components of x-ray scattering intensities, which are measured by the high-resolution double- and triple-crystal diffractometers, respectively, from imperfect films, multilayer structures, superlattices, etc. Examples of simulated rocking curves for the imperfect superlattice with defects of several types and reciprocal space map for the ion-implanted sample of yttrium iron garnet film with defects are given and discussed.

DOI: 10.1103/PhysRevB.99.235304

I. INTRODUCTION

The nondestructive x-ray diffraction methods are widely applied to determine characteristics of structural defects, chemical compositions, and strain distributions in various materials. The objects of such investigations are both the traditional as-grown and/or modified single-crystalline structures, as well as newly developed thin films, multilayer systems, superlattices, etc [1–5].

In particular, the measurements of rocking curves and reciprocal space maps in Bragg diffraction geometry, which make use of the high-resolution double- and triple-crystal diffractometers in combination with powerful x-ray sources, respectively, are the most effectively used experimental techniques (see, e.g., [Refs. [6–19]).

The efficiency of any x-ray diffraction method is determined to a large extent by the availability of the analytical expressions, which give an adequate description of measured rocking curves or reciprocal space maps. For this reason, the various theoretical models of x-ray diffraction were developed to analyze the diffraction patterns measured from perfect and imperfect crystalline bulk and multilayer structures with inhomogeneous strain distributions.

First of all, the x-ray diffraction models based on simple analytical expressions of the kinematical scattering theory should be mentioned. These models are devoted to perfect or almost perfect, i.e., nearly defect-free, thin multilayer systems or single-crystalline structures with smooth inhomogeneous strain fields [20,21]. In such approaches the alone parameter related to structural imperfection was the disorder factor caused by random static atom displacements. In addition, the more general kinematical diffraction formulas have been derived with the purpose of including a description of structure imperfections like random, continuous, or discrete fluctuations from the average superlattice parameters [22,23].

As a next step, the analytical solutions of dynamical Takagi-Taupin equations have been obtained for perfect multilayers in the semikinematical approximation [24–29]. Besides, the rigorous analytical solutions of these equations have been found in the cases of perfect crystals with strain fields of specific profile forms [30,31].

Within the scope of the purely dynamical consideration—which is necessary to describe x-ray diffraction by multilayer systems of the thickness exceeding an extinction length—the recurrence relations between coherent reflection coefficients of such systems, consisting of any number of layers with constant strains, have been derived by use of both Takagi-Taupin equations and Ewald-Bethe-Laue approaches [32–44].

Particularly, important generalizations of the dynamical theory have been made to include the cases of highly asymmetric and grazing-incidence and/or exit x-ray diffraction [41,42], extremal diffraction at Bragg angles near zero or $\pi/2$

*olikhovsky@meta.ua

[41,43], and wide-angle diffraction with a large number of Bragg reflections [44].

In addition, some approaches were proposed to solve analytically the inverse problem of x-ray scattering in Bragg diffraction geometry [45–47]. These approaches aimed to determine an arbitrary strain profile in crystal by using measured rocking curves, so the phase information was obtained in Ref. [45] from the observed reflection intensity via a logarithmic Hilbert transform to determine the strain distribution in a SiGe superlattice. A new numerical technique to compensate for the dynamical effects in experimental x-ray diffraction intensity profiles was proposed in Ref. [46], where an iterative algorithm of the strain determination in near-surface distorted layers was developed. The method based on the semidynamical approximation using the Fourier transform of the x-ray reflection amplitude was also proposed for the determination of depth-dependent strain distributions and static Debye-Waller factor of multilayer crystals from experimental x-ray diffraction data using an iteration algorithm [47].

It is important to emphasize that only in some of the above-mentioned theoretical approaches the influence of structure imperfections was taken into account via decreasing the coherent scattering amplitude due to a static Debye-Waller factor. However, all these approaches ignore the effect of immediate contribution of the diffuse scattering intensity from defects of real crystalline structures to measured x-ray diffraction intensity. However, this effect, together with an additional attenuation of the coherent scattering amplitude due to diffuse scattering, can cause substantial changes in the characterization results for strain parameters, chemical compositions, etc. Moreover, the application of diffuse scattering techniques has been proven to be an excellent tool for structural characterization of mesoscopic structures like superlattices with quantum dots, which enables one to investigate their shape, size, inner and outer strain fields, and positional correlation [3,4,48–51].

For this reason, the theoretical models of x-ray diffraction by multilayer systems or single-crystalline structures with inhomogeneous strain fields, which take the presence of randomly distributed defects into account, have been developed by using both kinematical and dynamical diffraction theories [1,3–5,50–60].

Particularly, the dynamical models were based either directly on Takagi equations [52] or on the differential version of Kato's statistical dynamical theory [51,53–60].

It is worth remarking that this differential version was formulated by Bushuev [61] to describe the angular diffraction intensity distributions in a case of incident plane wave, in contrast to the version formulated earlier by Kato [62] for an incident spherical wave which described the integrated diffraction intensities from imperfect crystals with mosaiclike structure only. These theoretical diffraction models were successfully used to treat the measurement data from imperfect crystal structures with heavy distortions caused by mosaiclike imperfections [58]. However, some difficulties are encountered when establishing quantitative relationships between the observed x-ray diffraction patterns and statistical characteristics of crystal imperfections like the randomly distributed defects with static Coulomb-type displacement fields, i.e., their size, concentration, strength, etc.

The origin of such kind of difficulties is that these models are fundamentally two dimensional; i.e., they consider the x-ray scattering processes exceptionally in the coherent diffraction plane. However, the correct quantitative description of the diffuse scattering processes from any type of randomly distributed finite-size defects, which always occur with photon momentum transfers in all three space dimensions, requires the corresponding three-dimensional (3D) space consideration. Moreover, also the second derivatives of wave field amplitudes in the wave equation, which are neglected in the so-called Takagi-Taupin approximation, where the smoothness of these amplitudes and strain fields at the distance of the extinction length was supposed, should be retained to consider correctly the behavior of coherent waves at layer interfaces with large strain gradients.

Presumably, just for these reasons a new formalism, based on the Dyson equation for the coherent wave field amplitude and Bethe-Salpeter equation for the incoherent (diffuse) scattering amplitude, has been proposed to describe the dynamical x-ray diffraction in statistically disturbed crystals [63,64].

It is remarkable that, perhaps for similar reasons, Kato also has reformulated his previous version of the statistical dynamical theory without using the Takagi-Taupin approximation on a physically sounder basis of the concept of the Green's function [65].

The above-mentioned difficulties are fundamentally absent in the generalized statistical dynamical theory of x-ray diffraction by imperfect single crystals with randomly distributed Coulomb-type defects [66,67].

This theory is based on the Ewald-Bethe-Laue approach [68], where the scattering problem is considered in the 3D momentum space, and makes use of the Krivoglaz method of fluctuating waves of defect concentration [69], which enables establishing direct analytical relationships between Fourier components of the fluctuating part of crystal polarizability and defect characteristics. In consequence, this theory provides the explicit analytical expressions in the 3D momentum space for coherent and diffuse scattering amplitudes with direct connections to statistical defect characteristics, which are well suited to be adopted for the description of the diffraction patterns measured by high-resolution double- and triple-crystal x-ray diffractometers (see, e.g., Refs. [70,71]).

The purpose of the present work is to extend the generalized statistical dynamical theory of x-ray diffraction by imperfect crystals with Coulomb-type defects [66,67] to the case of real single-crystalline multilayers of arbitrary thickness with inhomogeneous strain fields and randomly distributed defects.

The article has the following structure. In Sec. II, the main relations of the generalized statistical dynamical theory are briefly outlined for the case of Bragg diffraction geometry in imperfect crystals with randomly distributed Coulomb-type defects. In Sec. III, the recurrence relations are derived for the coherent amplitude reflection and transmission coefficients of the imperfect multilayer system consisting of any number of layers with nearly constant strains and randomly distributed defects in each one.

The analytical expression for the diffuse component of reflectivity of such systems, which is immediately connected with statistical characteristics of defects in each layer, is obtained in Sec. IV A. In addition, the corresponding expressions

are obtained for the diffuse scattering intensity distributions measured by the high-resolution double- (Sec. IV B) and triple-crystal diffractometers (Sec. IV C).

The derived formulas are used to simulate rocking curves for the imperfect InGaAs/GaAs superlattice with defects (Sec. V A) and a reciprocal space map for the imperfect epitaxial yttrium iron garnet film implanted with fluorine ions (Sec. V B), respectively. A short Summary and Conclusions are given in Sec. VI.

II. BASIC RELATIONS OF THE GENERALIZED STATISTICAL DYNAMICAL THEORY

A. Coherent scattering amplitude

Real single crystals, epitaxial films, and multilayer systems from the structural point of view are characterized by the presence of intrinsic point defects, growth defects, intentionally introduced impurities, inhomogeneous strain fields due to lattice misfits or composition variations, etc. If the thickness of any region of interest in such objects is comparable with the extinction length, the fully dynamical consideration is required for the correct interpretation of observed diffraction patterns, which always consist of coherent and diffuse components.

In the generalized statistical dynamical theory of x-ray scattering by imperfect single crystals with randomly distributed Coulomb-type defects [66,67] the perturbation method was applied to solve the wave equation in momentum space. The total polarizability of a crystal with randomly distributed defects was represented as the sum of average and fluctuating (random) parts. Similarly, the wave field in the crystal was subdivided into average and fluctuating parts, which correspond to coherent and diffusely scattered waves, respectively. Then the wave equation in momentum space could be solved separately for coherent and diffuse wave amplitudes.

Particularly, the coherent wave field in such imperfect crystals can be represented for each polarization state (σ and π) in two-beam approximation as a sum of transmitted $D_{\mathrm{T}}(\mathbf{r})$ and diffracted (scattered) $D_{\mathrm{S}}(\mathbf{r})$ waves:

$$D(\mathbf{r}) = D_{\mathrm{T}}(\mathbf{r}) + D_{\mathrm{S}}(\mathbf{r}), \tag{1}$$

$$D_{\mathrm{T}}(\mathbf{r}) = \sum_{\delta} D_0^{\delta} e^{-i\mathbf{K}_0^{\delta}\mathbf{r}}, \quad D_{\mathrm{S}}(\mathbf{r}) = \sum_{\delta} D_{\mathbf{H}}^{\delta} e^{-i\mathbf{K}_{\mathbf{H}}^{\delta}\mathbf{r}}, \tag{2}$$

where $\mathbf{r}$ is the space coordinate, $\mathbf{K}_0^{\delta}$ and $\mathbf{K}_{\mathbf{H}}^{\delta}$ in Eqs. (2) are wave vectors of strong Bragg waves, and $\delta = 1, 2$. The amplitudes of transmitted (D_0^{δ}) and diffracted ($D_{\mathbf{H}}^{\delta}$) coherent plane waves are found from the set of basic equations for the strong Bragg waves [66,67]:

$$\begin{aligned}(-2\varepsilon_0 + \chi_0 + \Delta\chi_{00})D_0 + (CE\chi_{-\mathbf{H}} + \Delta\chi_{0\mathbf{H}})D_{\mathbf{H}} = 0,\\ (CE\chi_{\mathbf{H}} + \Delta\chi_{\mathbf{H}0})D_0 + (-2\varepsilon_{\mathbf{H}} + \chi_0 + \Delta\chi_{\mathbf{HH}})D_{\mathbf{H}} = 0.\end{aligned} \tag{3}$$

Here ε_0 and $\varepsilon_{\mathbf{H}}$ are excitation errors, χ_0 and $\chi_{\pm\mathbf{H}}$ are Fourier components of the crystal polarizability, $C = 1$ or $\cos(2\theta_{\mathrm{B}})$ for σ and π polarization, respectively, θ_{B} is the Bragg angle, and $E = \exp(-L_{\mathbf{H}})$ is the static Krivoglaz-Debye-Waller factor. Complex dispersion corrections $\Delta\chi_{\mathbf{GG}'}$ appear due to diffuse scattering ($\mathbf{G}$ and $\mathbf{G}' = \mathbf{0}$ or $\mathbf{H}$, where $\mathbf{H}$ is the reciprocal lattice vector).

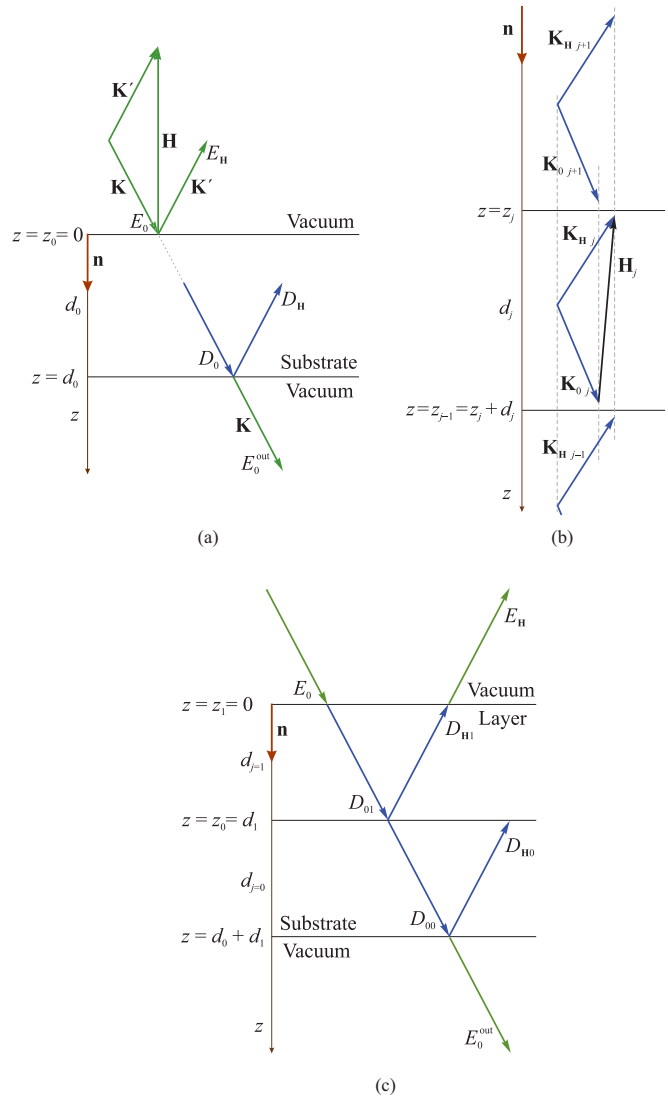

FIG. 1. Schematic diagram of relations between the wave vectors of incident, transmitted, and diffracted coherent plane waves in the single-crystal plate (a), arbitrary single layer of a multilayer crystal system (b), and epitaxial film on the substrate (c).

After solving the homogeneous equation set (3) and imposing boundary conditions at entrance and exit surfaces of the crystal plate of thickness d_0 [see Fig. 1(a)] we obtain the amplitudes of coherent plane waves constituting two dynamical wave fields:

$$D_0^{\delta} = (-1)^{\delta} E_0 \frac{B_{\delta'}}{B_1 - B_2}, \quad D_{\mathbf{H}}^{\delta} = c^{\delta} D_0^{\delta}, \tag{4}$$

$$B_{\delta} = c^{\delta} e^{-iK\Delta_{\delta} d_0}, \quad c^{\delta} = -\frac{-2\gamma_0\Delta_{\delta} + \chi_0 + \Delta\chi_{00}^{\delta}}{CE\chi_{-\mathbf{H}} + \Delta\chi_{0\mathbf{H}}^{\delta}}, \tag{5}$$

where E_0 is the amplitude of an incident plane wave with the wave vector $\mathbf{K}$, $K = 2\pi/\lambda$, λ is the x-ray wavelength, and $\delta' \neq \delta$.

Accommodations $\Delta_\delta = \varepsilon_0^\delta/\gamma_0$ of the wave vectors of strong Bragg waves, $\mathbf{K}_\mathbf{H}^\delta = \mathbf{K}_\mathbf{0}^\delta + \mathbf{H}$ and $\mathbf{K}_\mathbf{0}^\delta = \mathbf{K} + K\Delta_\delta \mathbf{n}$, which belong to the δth sheet of the dispersion surface, are described by the expression

$$\Delta_\delta = \frac{1}{2\gamma_0}\left(\chi_0 + \Delta\chi_{00}^\delta\right) + \frac{\lambda}{2\Lambda}[y + (-1)^\delta\sqrt{y^2-1}], \quad (6)$$

$$y = (\alpha - \alpha_0)\sqrt{b}/\sigma, \quad \Lambda = \lambda\sqrt{\gamma_0|\gamma_\mathbf{H}|}/\sigma, \quad (7)$$

$$\alpha = -\Delta\theta\sin 2\theta_\mathrm{B}, \quad 2\alpha_0 = \chi_0 + \Delta\chi_\mathbf{HH}^\delta + \left(\chi_0 + \Delta\chi_{00}^\delta\right)/b,$$

$$\sigma^2 = \left(CE\chi_\mathbf{H} + \Delta\chi_\mathbf{H0}^\delta\right)\left(CE\chi_{-\mathbf{H}} + \Delta\chi_\mathbf{H0}^\delta\right), \quad (8)$$

where $\mathbf{n}$ is the inner normal to the entrance crystal surface, Λ is the complex extinction length, $\Delta\theta$ is the angular deviation of the investigated crystal from the exact Bragg position, $b = \gamma_0/|\gamma_\mathbf{H}|$ is the parameter of diffraction asymmetry, and γ_0 and $\gamma_\mathbf{H}$ are direction cosines of wave vectors of incident and scattered ($\mathbf{K}'$) plane waves, respectively.

The amplitude $E_\mathbf{H}$ of the diffracted coherent plane wave in vacuum, which is generated by the crystal wave field $D_\mathrm{S}(\mathbf{r})$ can be found from the corresponding boundary condition at the entrance surface:

$$D_\mathrm{S}(\mathbf{r}) = E_\mathbf{H}\exp(-i\mathbf{K}'\mathbf{r})|_{z=0}, \quad (9)$$

$$\mathbf{K}' = \mathbf{K}_\mathbf{H}^\delta - K\varepsilon_\mathbf{H}^\delta\gamma_\mathbf{H}^{-1}\mathbf{n}, \quad (10)$$

$$\varepsilon_\mathbf{H}^\delta = \varepsilon_0^\delta\gamma_\mathbf{H}/\gamma_0 + \alpha. \quad (11)$$

Then, the normalized coherent scattering amplitude in the reflection direction can be written by using Eqs. (2), (4), (9), and (10) as follows:

$$r(\Delta\theta) = b^{-1/2}\frac{E_\mathbf{H}}{E_0} = \zeta b^{1/2}\frac{\mathrm{e}^{-iK\Delta_1 d_0} - \mathrm{e}^{-iK\Delta_2 d_0}}{B_1 - B_2},$$

$$\zeta = (CE\chi_\mathbf{H} + \Delta\chi_\mathbf{H0})(CE\chi_{-\mathbf{H}} + \Delta\chi_\mathbf{0H})^{-1}. \quad (12)$$

Similarly, after imposition of the boundary condition at the exit surface for the transmitted coherent plane wave in vacuum, which is generated by the crystal wave field $D_\mathrm{T}(\mathbf{r})$,

$$D_\mathrm{T}(\mathbf{r}) = E_0^\mathrm{out}\exp(-i\mathbf{K}\mathbf{r})|_{z=d_0}, \quad (13)$$

we obtain the normalized coherent scattering amplitude in the transmission direction:

$$t(\Delta\theta) = \frac{E_0^\mathrm{out}}{E_0} = e^{-iK(\Delta_1+\Delta_2)d_0}\frac{c^1 - c^2}{B_1 - B_2}. \quad (14)$$

The expressions for amplitude reflection (12) and transmission (14) coefficients are valid at arbitrary crystal thickness. These coefficients are related with characteristics of the crystal defect structure via both static Krivoglaz-Debye-Waller factor E and complex dispersion corrections to the wave vectors of strong Bragg waves due to diffuse scattering, $\Delta\chi_\mathbf{GG'}^\delta$. The latter can be subdivided into real and imaginary parts $\Delta\chi_\mathbf{GG'}^\delta = P_\mathbf{GG'}^\delta - i\mu_\mathbf{GG'}^\delta/K$ [66].

The coefficients of absorption due to diffuse scattering can be calculated in the case of Bragg diffraction geometry as follows [66,70]:

$$\mu_\mathbf{HH}(\Delta\theta) \approx \frac{C^2V}{4\lambda^2}\int_{K'=K} dS_{\mathbf{K}'}\, S(\mathbf{q})/K^2 \equiv \mu_\mathrm{ds}(\Delta\theta),$$

$$\mu_{00}(\Delta\theta) \approx b\mu_\mathbf{HH}(\Delta\theta),$$

$$\mu_\mathbf{0H}(\Delta\theta) \approx \mu_\mathbf{H0}(\Delta\theta) \approx \mu_\mathbf{HH}(\Delta\theta)R_\mathrm{eff}/(R_\mathrm{eff} + \mathrm{Re}\,\Lambda), \quad (15)$$

where $dS_{\mathbf{K}'} = K^2 d\Omega_{\mathbf{K}'}$ is the surface element on the Ewald sphere, which is perpendicular to the $\mathbf{K}'$ direction in reciprocal space. The correlation function $S(\mathbf{q}) \approx \mathrm{Re}\langle\delta\chi_{\mathbf{q}-\mathbf{H}+2\mathbf{G}}\delta\chi_{-\mathbf{q}+\mathbf{H}-2\mathbf{G}'}\rangle$ is dependent on Fourier components of the fluctuation part of crystal polarizability $\delta\chi_{\mathbf{G}+\mathbf{q}}$, where angular brackets denote averaging on the statistical ensemble of defects, and $\mathbf{q}$ is a complex momentum transfer. The expressions for absorption coefficient due to diffuse scattering $\mu_\mathrm{ds}(\Delta\theta)$ and the effective radius of a certain type of defects R_eff will be defined below in Secs. IV B and IV A, respectively. The real parts of the dispersion corrections $\Delta\chi_\mathbf{GG'}^\delta$ are approximately described by relations $P_\mathbf{GG'}^\delta(\Delta\theta) \approx K^{-1}\mu_\mathbf{GG'}^\delta(\Delta\theta)$ [66].

The expressions for $\Delta\chi_\mathbf{GG'}^\delta$ provide the possibility to perform correct calculations of angular dependencies of absorption effects because of diffuse scattering for strong Bragg waves in crystals with microdefects. The simultaneous presence of several types of defects in a crystal leads to summation of their contributions in corresponding formulas like equations for μ_ds and $L_\mathbf{H}$.

B. Dynamical diffuse scattering amplitude

Diffusely scattered waves are generated because of scattering of both strong Bragg (coherent) and diffusely scattered waves on the fluctuating part of the static displacement field of crystal atoms, which is caused by chaotically distributed defects. In crystal, analogously to coherent waves, the diffusely scattered waves form a dynamical wave field too. In the two-beam approximation of diffraction, the amplitudes of diffusely scattered plane waves $D_\mathbf{q}$ and $D_{\mathbf{H}+\mathbf{q}}$ satisfy the set of inhomogeneous equations [66,67]:

$$\left(-2\varepsilon_{0\mathbf{q}}^\delta + \chi_0 + \Delta\chi'^\delta_{00}\right)D_\mathbf{q} + \left(CE\chi_{-\mathbf{H}} + \Delta\chi'^\delta_{0\mathbf{H}}\right)D_{\mathbf{H}+\mathbf{q}}$$
$$= -\left(\delta\chi_\mathbf{q}D_0^\delta + C\delta\chi_{-\mathbf{H}+\mathbf{q}}D_\mathbf{H}^\delta\right),$$

$$\left(CE\chi_\mathbf{H} + \Delta\chi'^\delta_{\mathbf{H}0}\right)D_\mathbf{q} + \left(-2\varepsilon_{\mathbf{H}\mathbf{q}}^\delta + \chi_0 + \Delta\chi'^\delta_{\mathbf{HH}}\right)D_{\mathbf{H}+\mathbf{q}}$$
$$= -\left(C\delta\chi_{\mathbf{H}+\mathbf{q}}D_0^\delta + \delta\chi_\mathbf{q}D_\mathbf{H}^\delta\right), \quad (16)$$

where $\varepsilon_{0\mathbf{q}}^\delta$ and $\varepsilon_{\mathbf{H}\mathbf{q}}^\delta$ are the excitation errors of the diffusely scattered waves, $\delta\chi_{\mathbf{G}+\mathbf{q}}$ are the fluctuating Fourier components of the crystal polarizability ($\mathbf{G} = 0, \pm\mathbf{H}$), and $\Delta\chi'^\delta_\mathbf{GG'}$ are the dispersion corrections accounting for multiple diffuse scattering processes.

After solving the inhomogeneous equation set (16) and imposition of boundary conditions at entrance and exit surfaces of the crystal plate for Bragg diffraction geometry, one can find the dynamical diffuse scattering amplitudes in transmission ($\mathbf{G} = 0$) and diffraction ($\mathbf{G} = \mathbf{H}$) directions

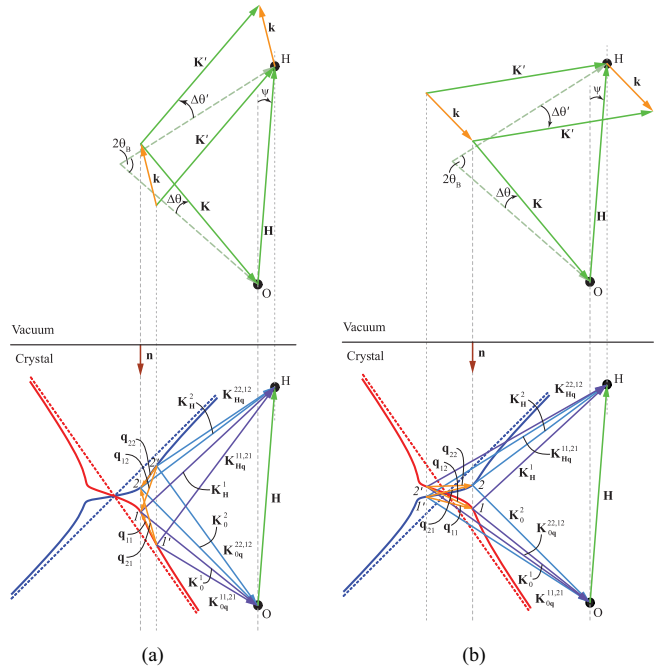

FIG. 2. Relations between the wave vectors of coherent ($\mathbf{K}_0^\delta$ and $\mathbf{K}_\mathbf{H}^\delta$) and diffusely scattered plane waves ($\mathbf{K}_0^\delta + \mathbf{q}_{\delta\tau}$ and $\mathbf{K}_\mathbf{H}^\delta + \mathbf{q}_{\delta\tau}$) with momentum transfers $\mathbf{q}_{\delta\tau}$ on dispersion branches for the asymmetric Bragg diffraction geometry of the absorbing crystal (Ge 333, Cu Kα_1, asymmetry angle $\psi = 5°$). Angular deviations $\Delta\theta$ and $\Delta\theta'$ of the wave vectors of incident ($\mathbf{K}$) and diffusely scattered ($\mathbf{K}'$) plane waves in vacuum, respectively, from their exact Bragg reflection directions (shown by dashed lines) lead to the deviation $\mathbf{k}$ of the $\mathbf{K}'$ vector from the reciprocal lattice point H. Two of four possible cases of the angular deviation combinations are shown: (a) $\Delta\theta > 0$ and $\Delta\theta' > 0$, and (b) $\Delta\theta > 0$ and $\Delta\theta' < 0$.

($\mathbf{G}' = 0$ and $\mathbf{H}$):

$$f_\mathbf{G}(\mathbf{K}', \mathbf{K}) = \sum_{\delta=1}^{2}\sum_{\tau=1}^{2}\sum_{\mathbf{G}'} D_{\mathbf{G}'}^{\delta} F_{\mathbf{G}\mathbf{G}'}^{\delta\tau}(\mathbf{q}_{\delta\tau}), \quad \mathbf{q}_{\delta\tau} = \mathbf{K}_{0\mathbf{q}}^{\delta\tau} - \mathbf{K}_0^\delta, \tag{17}$$

where $F_{\mathbf{G}\mathbf{G}'}^{\delta\tau}(\mathbf{q}_{\delta\tau})$ are the partial amplitudes of the scattering of strong Bragg plane waves with wave vectors $\mathbf{K}_0^\delta$ and $\mathbf{K}_\mathbf{H}^\delta$ into the diffuse ones within the crystal, having wave vectors $\mathbf{K}_{0\mathbf{q}}^{\delta\tau} = \mathbf{K}_0^\delta + \mathbf{q}_{\delta\tau}$ and $\mathbf{K}_{\mathbf{H}\mathbf{q}}^{\delta\tau} = \mathbf{K}_{0\mathbf{q}}^{\delta\tau} + \mathbf{H}$, respectively. The vectors $\mathbf{q}_{\delta\tau} = \mathbf{k} + K(\Delta'_\tau - \Delta_\delta)\mathbf{n}$ are the corresponding complex momentum transfers, $\Delta'_\tau = \varepsilon_{\mathbf{H}\mathbf{q}}^{\delta\tau}/\gamma_\mathbf{H}$ are the accommodations of the wave vectors of diffusely scattered waves, and the vector $\mathbf{k} = \mathbf{K}' - \mathbf{K} - \mathbf{H}$ determines the deviation of the wave vector $\mathbf{K}'$ of a diffusely scattered wave in vacuum from the reciprocal lattice point H (see Fig. 2). The hyperbola branches shown in Fig. 2 picture the result of the intersection of the dispersion surface sheets for diffusely scattered waves with the coherent scattering plane ($\mathbf{K}$, $\mathbf{H}$). It should also be remarked that the vectors $\mathbf{q}_{\delta\tau}$, $\mathbf{k}$, and $\mathbf{K}'$ have the components perpendicular to this plane; they not shown in Fig. 2. Moreover, the only real parts of the $\mathbf{q}_{\delta\tau}$ vectors are shown. Note also that for the sake of clarity we neglect possible differences because of different dispersion corrections between the branches of the dispersion surfaces for diffusely scattered waves and the same branches of the dispersion surface for coherent waves. Besides, the double superscript on the wave vectors of diffusely scattered waves shown in Fig. 2 was used to point out that both of these vectors are equal, i.e., $\mathbf{K}_{0\mathbf{q}}^{1\tau} = \mathbf{K}_{0\mathbf{q}}^{2\tau}$, etc., although obtained in two different ways: from the different wave vectors of strong Bragg waves and different momentum transfers, namely, $\mathbf{K}_{0\mathbf{q}}^{1\tau} = \mathbf{K}_0^1 + \mathbf{q}_{1\tau}$ and $\mathbf{K}_{0\mathbf{q}}^{2\tau} = \mathbf{K}_0^2 + \mathbf{q}_{2\tau}$, respectively.

The expression (17) can be simplified substantially in the limiting cases of thin or thick crystals ($\mu_0 d_0 \ll 1$ or $\mu_0 d_0 > 1$, respectively, where $\mu_0 = K|\chi_{i0}|$ is the photoelectric absorption coefficient). Thereby, for the diffuse scattering amplitude in the diffraction direction by supposing $\delta\chi_{-\mathbf{H}+\mathbf{q}} \approx -\delta\chi_{\mathbf{H}+\mathbf{q}}$ we approximately obtain

$$f_\mathbf{H}(\mathbf{K}', \mathbf{K}) \cong \frac{CVK^2}{4\pi} F^{\mathrm{dyn}}(\Delta\theta)\delta\chi_{\mathbf{H}+\mathbf{q}}. \tag{18}$$

Here, the dynamical factor F^{dyn} describes the modulation of diffuse scattering amplitude, which is caused by the interference of strong Bragg waves:

$$F^{\mathrm{dyn}}(\Delta\theta) = \begin{cases} 1 - \sqrt{\zeta b}\{y - \mathrm{sgn}[\mathrm{Re}(y)]\sqrt{y^2 - 1}\}, & \mu_0 d_0 \gg 1 \\ 1, & \mu_0 d_0 \ll 1 \end{cases}. \tag{19}$$

The interference absorption coefficient μ_i in the complex momentum transfer $\mathbf{q} = \mathbf{k} + i\mu_\mathrm{i}\mathbf{n}$ describes the extinction effect for diffusely scattered waves and is given by the relationship

$$\mu_\mathrm{i}(\Delta\theta, \Delta\theta') = \frac{\mu_0}{2\gamma_0}\frac{b+1}{2}\frac{E}{|g|}[r_i(z) + r_i(z')], \tag{20}$$

where the next notation was used:

$$r_i(z) = \sqrt{\frac{1}{2}(\sqrt{u^2 + v^2} - u)}, \quad u = (z^2 - g^2)E^{-2} + \text{æ}^2 - 1,$$
$$v = 2(zgE^{-2} - p),$$

$$z = \frac{\Delta\theta \sin(2\theta_\mathrm{B})}{C|\chi_{\mathrm{r}\mathbf{H}}|}\sqrt{b}, \quad z' = \frac{\Delta\theta' \sin(2\theta_\mathrm{B})}{C|\chi_{\mathrm{r}\mathbf{H}}|}\sqrt{b},$$
$$g = -\frac{|\chi_{i0}|}{|\chi_{\mathrm{r}\mathbf{H}}|}\frac{\sqrt{b} + 1/\sqrt{b}}{2C}, \quad \text{æ} = \frac{|\chi_{i\mathbf{H}}|}{|\chi_{\mathrm{r}\mathbf{H}}|},$$
$$p = \text{æ}\cos\nu_\mathbf{H}, \quad \cos\nu_\mathbf{H} = \frac{\chi'_{\mathrm{r}\mathbf{H}}\chi'_{\mathrm{i}\mathbf{H}} + \chi''_{\mathrm{r}\mathbf{H}}\chi''_{\mathrm{i}\mathbf{H}}}{|\chi_{\mathrm{r}\mathbf{H}}| \cdot |\chi_{i\mathbf{H}}|},$$
$$|\chi_{\mathrm{r}\mathbf{H}}| = \sqrt{\chi'^2_{\mathrm{r}\mathbf{H}} + \chi''^2_{\mathrm{r}\mathbf{H}}}, \quad |\chi_{i\mathbf{H}}| = \sqrt{\chi'^2_{\mathrm{i}\mathbf{H}} + \chi''^2_{\mathrm{i}\mathbf{H}}},$$

where $\chi'_{\mathrm{r}\mathbf{H}}$, $\chi'_{\mathrm{i}\mathbf{H}}$ and $\chi''_{\mathrm{r}\mathbf{H}}$, $\chi''_{\mathrm{i}\mathbf{H}}$ are real and imaginary parts of the Fourier components of the complex crystal polarizability $\chi = \chi_\mathrm{r} + i\chi_\mathrm{i}$, respectively.

The interference absorption coefficient (20) can be estimated as $\mu_i \sim \pi/\Lambda$ near the exact Bragg directions for the wave vectors of incident and diffracted plane waves, and as $\mu_i \sim \mu_0(b+1)/(2\gamma_0)$ beyond these directions. This coefficient is an analog of the artificial cutoff parameter in kinematical theory, which removes a nonphysical divergence at $k \to 0$ in kinematical expressions for diffuse scattering intensity distributions, but it appears within the dynamical theory in a natural way.

III. COHERENT COMPONENT OF THE DYNAMICAL REFLECTIVITY OF AN IMPRFECT MULTILAYER SYSTEM

A. Dynamical wave field in an arbitrary layer

The relatively simple analytical description of the dynamical x-ray diffraction in real imperfect multilayer systems with defects and inhomogeneous strain fields can be achieved due to their subdivision into virtual laminae with randomly distributed defects and constant average strain in each lamina, i.e., by using the so-called layer approximation. Then the recurrence relations between coherent components of amplitude reflection and transmission coefficients of such multilayer crystal system can be derived from the dynamical theory of x-ray diffraction by imperfect single crystals as well as the expression for the diffuse scattering amplitude [66,67,72].

Indeed, in accordance with Ewald-Bethe-Laue approach one can consider relations between the wave fields existing in each layer by imposing corresponding boundary conditions at the surfaces of adjacent layers. In the single crystal, which contains randomly distributed Coulomb-type defects (i.e., dilatation centers like point defects as well as two- and three-dimensional clusters, new phase particles, etc.), the wave field can be represented in the two-wave approximation as the sum of two transmitted and diffracted coherent plane waves and corresponding diffusely scattered ones. The coherent wave field in an arbitrary layer of the imperfect multilayer system can be written in a similar way.

Let the multilayer system consists of substrate ($j = 0$) and M layers ($j = 1$ to M), [see Fig. 1(b)], with randomly distributed defects in each layer. Then, in the case of Bragg diffraction geometry the coherent wave field in the jth layer, which is bounded by plane surfaces $z = z_j$ and $z = z_{j-1}$, can be written for each polarization state (σ and π) as follows ($\delta = 1$ and 2):

$$D_j(\mathbf{r}) = D_{\mathrm{T}j}(\mathbf{r}) + D_{\mathrm{S}j}(\mathbf{r}), \tag{21}$$

$$D_{\mathrm{T}j}(\mathbf{r}) = \sum_{\delta} D^{\delta}_{0j} \exp\left(-i\mathbf{K}^{\delta}_{0j}\mathbf{r}\right), \tag{22}$$

$$D_{\mathrm{S}j}(\mathbf{r}) = \sum_{\delta} D^{\delta}_{\mathbf{H}j} \exp\left(-i\mathbf{K}^{\delta}_{\mathbf{H}j}\mathbf{r}\right). \tag{23}$$

The wave vectors of transmitted ($\mathbf{K}^{\delta}_{0j}$) and diffracted ($\mathbf{K}^{\delta}_{\mathbf{H}j}$) coherent plane waves in Eqs. (22) and (23) can be represented as follows:

$$\begin{aligned} \mathbf{K}^{\delta}_{0j} &= \mathbf{K}_{0,j+1} + K_{j+1}\Delta^{j}_{\delta}\mathbf{n} \approx \mathbf{K}_{0,j+1} + K\Delta^{j}_{\delta}\mathbf{n}, \\ \mathbf{K}^{\delta}_{\mathbf{H}j} &= \mathbf{K}^{\delta}_{0j} + \mathbf{H}_j, \end{aligned} \tag{24}$$

where $K_{0,j+1} = K_{j+1} = K(1+\chi_{0,j+1})^{1/2} \approx K$ is the modulus of the wave vector of the plane wave incident on the jth layer with the reciprocal lattice vector $\mathbf{H}_j$. In turn, the wave vector of the plane wave outgoing from the jth layer back into the $(j+1)$th layer is defined as follows:

$$\mathbf{K}_{\mathbf{H},j+1} = \mathbf{K}^{\delta}_{\mathbf{H}j} - K_{j+1}\varepsilon^{\delta}_{\mathbf{H}j}\gamma_{\mathbf{H}}^{-1}\mathbf{n}, \tag{25}$$

$$\varepsilon^{\delta}_{\mathbf{H}j} = \varepsilon^{\delta}_{0j}\gamma_{\mathbf{H}}/\gamma_0 + \alpha_j, \quad \varepsilon^{\delta}_{0j} = \gamma_0\Delta^{j}_{\delta}. \tag{26}$$

Accommodations of the wave vectors of strong Bragg waves in the jth layer, $\mathbf{K}^{\delta}_{0j}$ and $\mathbf{K}^{\delta}_{\mathbf{H}j}$, are described by the expression

$$\begin{aligned} \Delta^{j}_{\delta} &= \frac{1}{2\gamma_0}\left(\chi_{0j} + \Delta\chi^{\delta}_{00j}\right) + \frac{\lambda}{2\Lambda_j}\left[y_j + (-1)^{\delta}\sqrt{{y_j}^2 - 1}\right], \\ \Lambda_j &= \lambda(\gamma_0|\gamma_{\mathbf{H}}|)^{1/2}/\sigma_j, \quad \sigma_j^2 = (CE_j\chi_{\mathbf{H}j} + \Delta\chi_{\mathbf{H}0j}) \\ &\quad \times (CE_j\chi_{-\mathbf{H}j} + \Delta\chi_{0\mathbf{H}j}), \end{aligned} \tag{27}$$

where the index j denotes the connection of the corresponding quantity with the jth layer.

The normalized angular deviation y_j in Eq. (27) is defined by deviations $\Delta\mathbf{H}$ of the reciprocal lattice vector of substrate $\mathbf{H} \equiv \mathbf{H}_0$ ($j = 0$) due to sample rotation and $\Delta\mathbf{H}_j$ of the reciprocal lattice vector $\mathbf{H}_j = \mathbf{H}_0 + \Delta\mathbf{H}_j$ due to the average strain caused by defects or chemical composition in the jth ($j = 1$ to M) layer different from that in substrate, respectively (see Fig. 3):

$$y_j = (\alpha_j - \alpha_{0j})\sqrt{b}/\sigma_j, \tag{28}$$

$$\begin{aligned} \alpha_j &= (\mathbf{K}_j + \mathbf{H}_j)(\Delta\mathbf{H} + \Delta\mathbf{H}_j)/{K_j}^2 \\ &\approx -(\Delta\theta + \Delta\theta_j)\sin(2\theta_{\mathrm{B}}), \\ \alpha_{0j} &= \frac{1}{2}\left[\chi_{0j} + \Delta\chi_{\mathbf{H}\mathbf{H}j} + \frac{1}{b}(\chi_{0j} + \Delta\chi_{00j})\right], \end{aligned} \tag{29}$$

$$\begin{aligned} \Delta\theta_j &= (\varepsilon^{j}_{\perp}\cos^2\psi + \varepsilon^{j}_{||}\sin^2\psi)\tan\theta_B + \mathrm{sgn}(1-b)(\varepsilon^{j}_{\perp} - \varepsilon^{j}_{||}) \\ &\quad \times \sin\psi\,\cos\psi, \end{aligned} \tag{30}$$

where $\Delta\theta \approx \Delta H/H$ (with $\Delta\mathbf{H}\perp\mathbf{H}$) is the angular deviation of the substrate from the exact Bragg position due to sample rotation, $\Delta\theta_j$ is the angular deviation of the jth layer from the substrate orientation due to the strain, $\varepsilon^{j}_{\perp}$ and $\varepsilon^{j}_{||}$ are normal and parallel strain components in the jth layer, and ψ is the angle between the crystal surface and reflecting planes. It should be emphasized that the additional average strain in the jth layer can be caused not only by differences in chemical composition of layers but also due to randomly distributed defects of various types.

B. Recurrence relation for amplitude reflection coefficients

Consider now x-ray diffraction in the system consisting of a substrate ($j = 0$) and only one layer ($j = 1$) [see Fig. 1(c)]. Amplitudes of the transmitted and diffracted coherent waves, which form the coherent wave field in this layer for each polarization state, i.e., σ and π, can be found from the boundary conditions for all the waves entering into the layer from

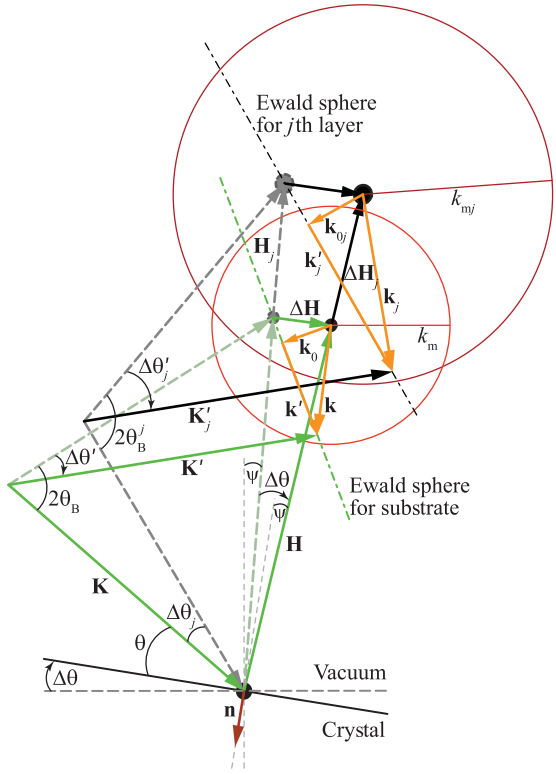

FIG. 3. Schematic plot of the integration path of the diffuse scattering intensity in a momentum space, where the dash-dotted line represents the intersection of the coherent scattering plane ($\mathbf{K}$, $\mathbf{H}$) with the integration plane tangent to the Ewald sphere, and $\mathbf{k}_{0j}$ is the deviation of the Ewald sphere from the reciprocal lattice point $\mathbf{H}_j$. At $|\mathbf{k}_{0j}| \leqslant k_{mj}$ the integration area includes both Huang ($|\mathbf{k}_{0j} + \mathbf{k}'| \leqslant k_{mj}$) and Stokes-Wilson ($|\mathbf{k}_{0j} + \mathbf{k}'| \geqslant k_{mj}$) scattering regions.

both its sides, i.e., from the entrance ($z_1 = 0$) and substrate ($z_0 = z_1 + d_1$) surfaces:

$$D_{T1}(\mathbf{r}) = \sum_\delta D^\delta_{01} e^{-i\mathbf{K}^\delta_{01}\mathbf{r}} = E_0 e^{-i\mathbf{K}\mathbf{r}}|_{z=z_1},$$
$$D_{S1}(\mathbf{r}) = \sum_\delta D^\delta_{\mathbf{H}1} e^{-i\mathbf{K}^\delta_{\mathbf{H}1}\mathbf{r}} = D^{\text{out}}_{\mathbf{H}0} e^{-i\mathbf{K}_{\mathbf{H}1}\mathbf{r}}|_{z=z_0}, \quad (31)$$

where $D^{\text{out}}_{\mathbf{H}0}$ is the amplitude of the diffracted coherent wave outgoing from the substrate, and the wave vectors of transmitted and diffracted coherent waves in the layer are connected with the wave vector of the diffracted coherent wave in vacuum $\mathbf{K}'$ via the relation

$$\mathbf{K}^\delta_{\mathbf{H}1} = \mathbf{K}' + K\varepsilon^\delta_{\mathbf{H}1}\gamma^{-1}_{\mathbf{H}}\mathbf{n} = \mathbf{K}' + K\Delta^1_\delta\mathbf{n} + K\alpha_1\gamma^{-1}_{\mathbf{H}}\mathbf{n}. \quad (32)$$

After substituting Eqs. (22)–(24) into the equation set (31), supposing $\mathbf{K}_{\mathbf{H}1} \approx \mathbf{K}'$ and accounting for the equality of tangential components of the wave vectors at the layer interfaces, we obtain the following equation set:

$$D^1_{01} + D^2_{01} = E_0,$$
$$c^1_1 D^1_{01} e^{-iK\Delta^1_1 d_1} + c^2_1 D^2_{01} e^{-iK\Delta^1_2 d_1} = D^{\text{out}}_{\mathbf{H}0} e^{iK\alpha_0\gamma^{-1}_{\mathbf{H}}d_1}. \quad (33)$$

The solution of the equation set (33) gives the amplitudes of the wave field in the layer:

$$D^\delta_{01} = (-1)^\delta \frac{E_0 B^1_{\delta'} - D^{\text{out}}_{\mathbf{H}0} e^{iK\alpha_0\gamma^{-1}_{\mathbf{H}}d_1}}{B^1_1 - B^1_2}, \quad (34)$$
$$B^j_\delta = c^\delta_j e^{-iK\Delta^j_\delta d_j}, \quad (35)$$

where the relations known from the generalized statistical dynamical theory of x-ray diffraction by imperfect single crystals were taken into account [66] [cf. Eqs. (4)–(6)]:

$$D^\delta_{\mathbf{H}\,j} = c^\delta_j D^\delta_{0j}, \quad (36)$$
$$c^\delta_j = (\zeta_j b)^{1/2}\left[y_j + (-1)^\delta\sqrt{y_j{}^2 - 1}\right]. \quad (37)$$

Now one can determine the amplitudes of the transmitted and diffracted coherent waves outgoing from the layer into the substrate and vacuum, respectively, by substituting Eq. (34) into the corresponding boundary conditions:

$$D_{T1}(\mathbf{r}) = \sum_\delta D^\delta_{01} e^{-i\mathbf{K}^\delta_{01}\mathbf{r}} = D^{\text{out}}_{01} e^{-i\mathbf{K}_{00}\mathbf{r}}|_{z=z_0}, \quad (38)$$
$$D_{S1}(\mathbf{r}) = \sum_\delta D^\delta_{\mathbf{H}1} e^{-i\mathbf{K}^\delta_{\mathbf{H}1}\mathbf{r}} = E_{\mathbf{H}} e^{-i\mathbf{K}'\mathbf{r}}|_{z=z_1}. \quad (39)$$

By using the expressions for the wave vectors of diffracted coherent plane waves (25) and approximate relation $K_{\mathbf{H},j-1} = K_{j-1} = K(1 + \chi_{0,j-1})^{1/2} \approx K$, Eqs. (38) and (39) can be reduced to the following form:

$$D^1_{01} e^{-iK\Delta^1_1 d_1} + D^2_{01} e^{-iK\Delta^1_2 d_1} = D^{\text{out}}_{01}, \quad (40)$$
$$c^1_1 D^1_{01} + c^2_1 D^2_{01} = E_{\mathbf{H}}. \quad (41)$$

Substituting Eq. (34) into Eqs. (40) and (41), we obtain the amplitude of the transmitted coherent plane wave outgoing from the layer, which is incident on the substrate, and the amplitude of the coherent plane wave, which is diffracted by the system of one layer on the substrate, respectively:

$$D^{\text{out}}_{01} = E_0 t_1 + D^{\text{out}}_{\mathbf{H}0} e^{iK\alpha_0\gamma^{-1}_{\mathbf{H}}d_1}\frac{r_1}{\zeta_1\sqrt{b}}, \quad (42)$$
$$E_{\mathbf{H}} = E_0\sqrt{b}r_1 + \frac{t_1}{e_1} D^{\text{out}}_{\mathbf{H}0} e^{iK\alpha_0\gamma^{-1}_{\mathbf{H}}d_1}. \quad (43)$$

Here, the quantities r_j and t_j are the amplitude reflection and transmission coefficients of the jth layer, respectively:

$$r_j = \zeta_j b^{1/2}\frac{e^{-iK\Delta^j_1 d_j} - e^{-iK\Delta^j_2 d_j}}{B^j_1 - B^j_2}, \quad (44)$$
$$t_j = e_j\frac{c^1_j - c^2_j}{B^j_1 - B^j_2}, \quad (45)$$
$$e_j = \exp\left[-iK\left(\Delta^j_1 + \Delta^j_2\right)d_j\right]. \quad (46)$$

Both the expressions (42) and (43) involve the amplitude of the coherent plane wave, which is diffracted by the substrate,

$D_{\mathbf{H}0}^{\text{out}}$. This amplitude can be found in two steps. First, as far as the amplitude of the coherent plane wave incident on the substrate is known, $D_{00}^{\text{in}} \equiv D_{10}^{\text{out}}$, one can write, accounting for the definition of substrate reflectivity in Eq. (12),

$$D_{\mathbf{H}0}^{\text{out}} e^{iK\alpha_0\gamma_{\mathbf{H}}^{-1}d_1} = \sqrt{b}r_0 D_{00}^{\text{in}}. \tag{47}$$

Second, substituting Eq. (42) into this expression, we obtain the equation with respect to the unknown amplitude $D_{\mathbf{H}0}^{\text{out}}$:

$$D_{\mathbf{H}0}^{\text{out}} e^{iK\alpha_0\gamma_{\mathbf{H}}^{-1}d_1} = \sqrt{b}r_0\left(E_0 t_1 + D_{\mathbf{H}0}^{\text{out}} e^{iK\alpha_0\gamma_{\mathbf{H}}^{-1}d_1}\frac{r_1}{\zeta_1\sqrt{b}}\right). \tag{48}$$

The solution of Eq. (48) has the following form:

$$D_{\mathbf{H}0}^{\text{out}} = E_0\sqrt{b}r_0\frac{t_1}{1-\zeta_1{}^{-1}r_1r_0}e^{-iK\alpha_0\gamma_{\mathbf{H}}^{-1}d_1}. \tag{49}$$

After substituting Eq. (49) into Eq. (43) and by using the amplitude reflectivity definition in Eq. (12) we obtain the relationship between the amplitude reflection coefficients of the imperfect one-layer system R_1 and substrate r_0:

$$R_1 = r_1 + \frac{e_1{}^{-1}t_1{}^2 r_0}{1-\zeta_1{}^{-1}r_1r_0}. \tag{50}$$

The above-described procedure of matching the wave fields in the adjacent layers can be continued by adding a new upper layer and considering the one-layer system as a new substrate with amplitude reflection coefficient (50) and so on. Thus, we can obtain the recurrence relation between coherent amplitude reflection coefficients of two imperfect multilayer systems consisting of any number of M and $M-1$ layers for the case of arbitrary asymmetrical Bragg diffraction geometry:

$$R_j = \frac{r_j + R_{j-1}\left(e_j{}^{-1}t_j{}^2 - \zeta_j{}^{-1}r_j{}^2\right)}{1-\zeta_j{}^{-1}r_jR_{j-1}}, \tag{51}$$

where $j = 1$ to M, and $R_0 \equiv r_0$.

The dynamical amplitude reflection and transmission coefficients of the jth layer in Eq. (51) can be rewritten in the alternative form after substituting Eqs. (27), (35), and (37) into Eqs. (44) and (45):

$$r_j = \sqrt{\zeta_j}\left[y_j + i\sqrt{y_j{}^2-1}\cot\left(A_j\sqrt{y_j{}^2-1}\right)\right]^{-1}, \tag{52}$$

$$t_j = \sqrt{e_j}\left[\cos\left(A_j\sqrt{y_j{}^2-1}\right) - i\frac{y_j}{\sqrt{y_j{}^2-1}} \times \sin\left(A_j\sqrt{y_j{}^2-1}\right)\right]^{-1}. \tag{53}$$

Here, the notation $A_j = \pi d_j/\Lambda_j$ was used, and the amplitude absorption and phase factor (46) was rewritten as follows:

$$e_j = \exp\left[-iK\left(\chi_{0j} + \Delta\chi_{00j}^{\delta}\right)d_j/\gamma_0 - 2iA_jy_j\right]. \tag{54}$$

The structure of formula (51) is similar to that of the known recurrence relation for perfect multilayer systems with different strains in the layers [34,36,39]. The main difference is that the dynamical amplitude reflection and transmission coefficients in Eq. (51) take into account the influence of additional strain due to randomly distributed defects in the imperfect layers and substrate, as well as the absorption effects due to diffuse scattering.

Thus, the coherent component of reflectivity for the imperfect multilayer crystal system, which consists of M layers with randomly distributed defects, can be represented in the two-wave approximation for Bragg diffraction geometry as follows:

$$R_{\text{coh}}(\Delta\theta) = |R_M(\Delta\theta)|^2. \tag{55}$$

Here, the amplitude reflectivity of the upper Mth layer $R_M(\Delta\theta)$ is determined by using the recurrence relation (51) starting from the amplitude reflection coefficient of the substrate. The latter can be written according to Eq. (52) for the sufficiently thick substrate (i.e., at $\mu_0^0 d_0 \gg 1$, where μ_0^0 is the photoelectric absorption coefficient in substrate) as

$$r_0(y_0) \approx \sqrt{\zeta}[y_0 - \text{sgn}(y_{0\text{r}})\sqrt{y_0{}^2-1}]. \tag{56}$$

Here, the quantity y_0 denotes the normalized angular deviation of the substrate from its exact Bragg reflection position [see Eq. (28), $j=0$]; quantities $y_{0\text{r}} = \text{Re}y_0$ and $y_{0\text{i}} = \text{Im}y_0$ are the real and imaginary parts of y_0, respectively.

C. Recurrence relation for amplitude transmission coefficients

The derivation of the recurrence relation between the coherent amplitude transmission coefficients of the imperfect multilayer system can be carried out in the same way as described above for the reflection coefficients. Namely, the amplitude transmission coefficient of the one-layer system T_1 can be determined by using the definition of amplitude transmission coefficient in Eq. (14):

$$T_1 = E_0^{\text{out}}/E_0 = D_{00}^{\text{in}}t_0/E_0, \tag{57}$$

where the amplitude of the plane wave incident on the substrate can be determined by substituting Eq. (49) into Eq. (42) with account for the identity relation $D_{00}^{\text{in}} \equiv D_{10}^{\text{out}}$:

$$D_{00}^{\text{in}} = E_0\frac{t_1}{1-\zeta_1{}^{-1}r_1r_0}. \tag{58}$$

Then, after substituting Eq. (58) into Eq. (57), we obtain the relationship between the amplitude transmission coefficients of the imperfect one-layer system and substrate:

$$T_1 = \frac{t_1t_0}{1-\zeta_1{}^{-1}r_1r_0}. \tag{59}$$

Further, the recurrence relation between coherent amplitude transmission coefficients of two imperfect multilayer systems consisting of any number of M and $M-1$ layers can be written as follows:

$$T_j = \frac{t_jT_{j-1}}{1-\zeta_j{}^{-1}r_jR_{j-1}}, \tag{60}$$

where $j = 1$ to M, $T_0 \equiv t_0$, and $R_0 \equiv r_0$.

It should be noted here that this relation can be useful in the interpretation of the experimental observations like those reported in Ref. [73] for epitaxial CdF_2/CaF_2 superlattices investigated at Laue and Bragg diffraction geometries. It is important to emphasize that in such kind of measurements both reflection and transmission coefficients in Bragg diffraction geometry contain the information on defect characteristics

and, consequently, both ones can be used to analyze x-ray diffraction measurements.

However, it is more important to point out here that the majority of x-ray diffraction measurements on various multilayer structures have been performed in Bragg diffraction geometry (see, e.g., Refs. [1–6,8–16,48–51]), and, that the availability of the analytical expressions connecting the coherent component of reflection and transmission coefficients with statistical characteristics of defects in each layer via both static Krivoglaz-Debye-Waller factor and coefficient of absorption due to diffuse scattering can be useful for the quantitatively correct interpretation of such measurements.

IV. DIFFUSE COMPONENT OF REFLECTIVITY FOR AN IMPERFECT MULTILAYER SYSTEM

A. Differential diffuse scattering intensity

As can be seen from Eq. (17), the coherent waves with amplitudes $D^{\delta}_{\mathbf{G}}(\Delta\theta)$ are the sources of diffusely scattered waves. Therefore, the expression for the diffuse scattering amplitude from the jth layer in the imperfect multilayer crystal system also can be written similarly:

$$f_{\mathbf{H}_j}(\boldsymbol{K}', \boldsymbol{K}) = F_j^{\mathrm{abs}} \sum_{\delta} \sum_{\mathbf{G}_j} D^{\delta}_{\mathbf{G}_j}(\Delta\theta) F^{\delta}_{\mathbf{H}_j\mathbf{G}_j}(\mathbf{k}), \tag{61}$$

where $\mathbf{G}_j = 0, \mathbf{H}_j$, $F_M^{\mathrm{abs}} = 1$, and the absorption of transmitted and scattered waves in the layers lying above the jth layer is described at $j = 0$ to $(M-1)$ by the factor

$$F_j^{\mathrm{abs}} = \sum_{i=j+1}^{M} \exp(-\mu_i d_i). \tag{62}$$

The normal absorption coefficient in Eq. (62) includes both the linear photoelectric absorption coefficient μ_0^j and the absorption coefficient due to diffuse scattering in the jth layer:

$$\mu_j = \frac{1}{2}\left(\mu_0^j + \mu_{\mathrm{ds}}^j\right)\left(\frac{1}{\gamma_0} + \frac{1}{|\gamma_{\mathbf{H}}|}\right). \tag{63}$$

If the correlation between defect distributions in different layers is absent, then the diffuse component of differential reflectivity of the multilayer system can be represented as

$$R_{\mathrm{DS}}(\mathbf{k}) = \frac{1}{\gamma_0 S |E_0|^2} \sum_{j=0}^{M} \left\langle |f_{\mathbf{H}_j}|^2 \right\rangle_j, \tag{64}$$

where angular brackets denote averaging over a random distribution of defects in the jth layer, and S is the entrance surface area of the crystal. Substituting Eq. (61) into Eq. (64) and using the simplified expression (18) for the dynamical diffuse scattering amplitude, we obtain

$$R_{\mathrm{DS}}(\mathbf{k}) \approx \frac{1}{\gamma_0 S}\left(\frac{CK^2}{4\pi}\right)^2 \sum_{j=0}^{M} F_j^{\mathrm{abs}} F_j^{\mathrm{dyn}} V_j{}^2 \left\langle |\delta\chi_{\mathbf{H}_j+\mathbf{q}}|^2 \right\rangle_j, \tag{65}$$

where $V_j = Sd_j$, and the factor of the dynamical modulation of diffuse scattering amplitude in the jth layer, F_j^{dyn}, is described by Eq. (19) where all the parameters are related to this layer.

To perform in Eq. (65) averaging over a random distribution of defects of a certain type in the jth layer we use the method of fluctuation waves of defect concentration [69], according to which, at small defect concentration $c_j \ll 1$ the approximate expression is valid in the Huang scattering region, i.e., at $k \ll k_{\mathrm{m}j}$,

$$\delta\chi_{\mathbf{H}_j+\mathbf{q}} \approx iE_j\chi_{\mathbf{H}_j}(\mathbf{H}_j\mathbf{U}_{j\mathbf{q}})c_{j\,\mathbf{q}}, \tag{66}$$

where Fourier components of fluctuating defect concentration and static atom displacement field caused by a single defect of a certain type in the jth layer are defined as follows:

$$c_{j\,\mathbf{q}} = \frac{1}{N_j}\sum_{t=1}^{N_j}(c_{tj} - c_j)\exp(i\mathbf{q}\mathbf{R}_{tj}),$$

$$\mathbf{U}_{j\mathbf{q}} = \frac{1}{v_{\mathrm{c}}}\int \mathrm{d}\mathbf{r}\mathbf{U}_j(\mathbf{r})\exp(i\mathbf{q}\mathbf{r}).$$

Here, N_j is the number of unit cells in layer j; v_{c} is the unit cell volume; $\mathbf{R}_{tj}$ is a radius vector of an atom in the unit cell with number t in layer j, in which the center of the defect is located; the random number $c_{tj} = 1$ for the last case, and $c_{tj} = 0$ otherwise.

The quantity $k_{\mathrm{m}j} = 1/R_{\mathrm{eff}}^j$ gives the boundary $k = k_{\mathrm{m}j}$ between Huang and Stokes-Wilson scattering regions in layer j [67,70]. In Fig. 3, this boundary is described by the red circle with larger radius, which is determined by small defects in the jth layer. The red circle with a smaller radius k_{m} describes the corresponding boundary for large defects in the substrate ($j = 0$). Here, the effective radii of defects are defined as $R_{\mathrm{eff}} = E\sqrt{HA_{\mathrm{C}}}$ and $R_{\mathrm{eff}} = ER_L\sqrt{H|\mathbf{b}|}$ for clusters and dislocation loops, respectively, where $A_{\mathrm{C}} = \Gamma\varepsilon R_{\mathrm{C}}^3$ is the cluster strength, $\Gamma = (1+\nu)(1-\nu)^{-1}/3$, ν is the Poisson ratio, ε is the strain at the cluster boundary, R_{C} is the cluster radius, $\mathbf{b}$ is the Burgers vector, and R_{L} is the dislocation loop radius (the index j was dropped for brevity).

After averaging over a random distribution of defects in Eq. (65), we obtain, approximately

$$R_{\mathrm{DS}}(\mathbf{k}) \approx c_j\, v_{\mathrm{c}} \frac{(\pi C E_j |\chi_{\mathbf{H}_j}|)^2}{\gamma_0\lambda^4} \sum_{j=0}^{M} F_j^{\mathrm{abs}} F_j^{\mathrm{dyn}} F_j(\mathbf{q}) p_j(d_j)\, d_j, \tag{67}$$

The effective layer thickness, where the diffuse scattering intensity is formed, is controlled by the factor

$$p_j(d_j) = \frac{1 - \exp(-2\mu_{i\,j}\, d_j)}{2\mu_{i\,j} d_j}. \tag{68}$$

In Eq. (67), the following notation was used,

$$F_j(\mathbf{q}) = F_j^H(\mathbf{q}) \equiv |\mathbf{H}_j\mathbf{U}_{j\mathbf{q}}|^2, \tag{69}$$

which is supposed to be valid only in the Huang scattering region at $k \leqslant k_{\mathrm{m}j}$.

Equation (69) holds for spherically symmetric clusters. In the case of dislocation loops with asymmetric displacement fields Eq. (67) should be averaged over random orientations of Burgers vectors. Then, after spherical averaging over such orientations [74], Eq. (69) can be rewritten in the form

describing the diffuse scattering from both types of defects:

$$F_j(\mathbf{q}) = F_j^H(\mathbf{q}) \equiv {H_j}^2\left(B_1 + B_2\frac{\left|\mathbf{H}_j^0\mathbf{q}\right|^2}{|\mathbf{q}|^2}\right)\frac{1}{|\mathbf{q}|^2}, \tag{70}$$

where $\mathbf{H}_j^0 = \mathbf{H}_j/H_j$ is the unit vector. The parameters in Eq. (70) are defined for spherical clusters as follows:

$$B_1 = 0, \quad B_2 = (4\pi A_{\mathrm{C}}/v_{\mathrm{c}}). \tag{71}$$

For dislocation loops, the definitions hold:

$$B_1 = 4\left(\pi|\mathbf{b}|R_{\mathrm{L}}^2/v_{\mathrm{c}}\right)^2/15, \quad B_2 = \beta B_1,$$
$$\beta = (3\nu^2 + 6\nu - 1)(1-\nu)^{-2}/4, \tag{72}$$

(the index j at the parameters was dropped here for brevity).

To extend the consideration of momentum transfers $\mathbf{k}$ up to include the Stokes-Wilson scattering region, i.e., the region of asymptotic diffuse scattering at $k \gg k_{\mathrm{m}j}$, the expression in Eq. (70) should be replaced by the following one [67,70]:

$$F_j(\mathbf{q}) = F_j^{\mathrm{SW}}(\mathbf{q}) \equiv F_j^{\mathrm{H}}(\mathbf{q})k_{\mathrm{m}j}^2/|\mathbf{q}|^2. \tag{73}$$

In such a way the correct description of the asymptotic behavior of the differential diffuse scattering intensity in both Huang ($\sim 1/k^2$) and Stokes-Wilson ($\sim 1/k^4$) scattering regions is achieved; in addition the continuous matching of this intensity at the boundary between these regions is provided.

The approach for the calculation of diffuse scattering intensity from defects, which was described above, can be used to analytically estimate the thermal diffuse scattering intensity distribution. Such simplified model can be used, when the consideration is restricted to the sufficiently close vicinity of the reciprocal lattice point considered, where the condition $\hbar\omega_{\mathbf{q}}/k_{\mathrm{B}}T \ll 1$ holds [70].

At such condition, the only acoustic branch of phonon dispersion relations can be considered and the phonon frequency can be calculated as $\omega_{\mathbf{q}} = v_{\mathrm{S}}q$, where v_{S} is a phonon velocity [75]. The expression for the thermal diffuse scattering intensity can be reduced then to an analytical form, which is similar to that for spherical clusters and has the only distinction that the constants in Eq. (70) are put equal to $B_1 = k_{\mathrm{B}}T/(mv_{\mathrm{S}}^2)$ and $B_2 = 0$, where m is an atom mass [70].

Here, this approach was slightly modified for the application to crystal structures with the complicated basis consisting of different atoms. Namely, when, for example, the GaAs structure is considered, for the "effective clusters" of two types—which replace all the actual atoms in the Ga and As sublattices, respectively—the radii R_{C} were chosen of the order of atomic size. The quantitative criterion for determining the values of these radii was chosen such that calculated static Krivoglaz-Debye-Waller factors $E = \exp(-L_{\mathbf{H}})$ for each atom sort were equal to the corresponding thermal Debye-Waller factors $E = \exp(-M_{\mathbf{H}})$. The latter ones were calculated by using the known Debye-Waller B coefficients (B factor), which have been found for Ga and As atoms in GaAs crystals at room temperature [76], by using relationships for crystals with a cubic lattice:

$$M_{\mathbf{H}} = \beta(h^2 + k^2 + l^2), \quad \beta = \frac{B}{4a^2},$$

where h, k, l are Miller indices and a is the lattice parameter.

Herewith, the value of "strain" ε at such "cluster" boundary was put equal to $\langle u^2\rangle^{1/2}/R_C$, where $\langle u^2\rangle^{1/2}$ is the root-mean-square displacement of vibrating atoms. The last was found from the same B coefficients by using the known relationship in the isotropic approximation for cubic crystals $B = 8\pi^2\langle u^2\rangle/3$ (see, e.g., Ref. [77]). At the same time, the exponent of static Krivoglaz-Debye-Waller factor $E = \exp(-L_{\mathbf{H}})$ should be put to zero in the case, when the thermal diffuse scattering intensity distributions are calculated by using the final expressions in Secs. III B and IV B, for the purpose of avoiding the double use of the thermal Debye-Waller factor, which already is included in the structure factor and corresponding Fourier component of the crystal polarizability.

B. Diffuse scattering intensity integrated over Ewald sphere

When the rocking curve of the imperfect multilayer system is measured by the high-resolution double-crystal diffractometer with widely open detector window, the diffracted x-ray intensity is integrated over exit angles, i.e., over the Ewald sphere near the considered reciprocal lattice point H. The corresponding "integral" diffuse component of the measured reflection coefficient can be determined as follows:

$$R_{\mathrm{diff}}(\Delta\theta) = \int_{K'=K} R_{\mathrm{DS}}(\mathbf{k})\mathrm{d}\Omega_{\mathbf{K}'} \tag{74}$$

where $\mathrm{d}\Omega_{\mathbf{K}'}$ is a solid angle in the $\mathbf{K}'$ direction.

To perform the integration in Eq. (74), where the integrand is given by Eq. (67), one should replace the Ewald sphere near the considered reciprocal lattice point H by a plane tangent to the Ewald sphere at the endpoint of the wave vector $\mathbf{K}'$ (in the case $k \ll K'$). Then an element of surface area in Eq. (74) $\mathrm{d}S_{\mathbf{K}'} = K^2\mathrm{d}\Omega_{\mathbf{K}'}$ can be replaced by a plane two-dimensional area element $d\mathbf{k}'$ of the reciprocal space. Further, the momentum transfer $\mathbf{k}$ can be decomposed into the components parallel ($\mathbf{k}_0$) and perpendicular ($\mathbf{k}'$) to the wave vector $\mathbf{K}'$ (see Fig. 3). Then for any jth layer the relation $\mathbf{k} = \mathbf{k}_{0j} + \mathbf{k}'$ holds, and the integration over $\mathbf{k}'$ can be performed in the polar coordinate system chosen in the plane tangent to the Ewald sphere. Thus, we obtain the diffuse component of the rocking curve measured by the high-resolution double-crystal diffractometer with widely open detector window:

$$R_{\mathrm{diff}}(\Delta\theta) = \sum_{j=0}^{M} F_j^{\mathrm{ext}}F_j^{\mathrm{abs}}R_{\mathrm{diff}}^j(\Delta\theta). \tag{75}$$

As can be seen, the integral diffuse component of the reflectivity of the imperfect multilayer system in Eq. (75) appears to be the sum of corresponding integral diffuse components of all the layers with weight coefficients accounting for absorption and extinction. It should be emphasized that, in turn, the integral diffuse component of the reflectivity of the jth layer is proportional to the absorption coefficient due to diffuse scattering from defects in this layer:

$$R_{\mathrm{diff}}^j(\Delta\theta) = \mu_{\mathrm{ds}}^j(k_{0j})p_j'(d_j)d_j/\gamma_0. \tag{76}$$

If the substrate is thick ($\mu_0 d_0 \gg 1$) and layers are thin ($\mu_j d_j \ll 1$, $j = 1$ to M), the diffuse reflectivities in Eq. (76)

can be represented as follows:

$$R^0_{\rm diff} = \frac{\mu^0_{\rm ds}(\Delta\theta)}{(1+b)\mu^0_0}, \quad R^j_{\rm diff} = \frac{\mu^j_{\rm ds}(\Delta\theta)d_j}{\gamma_0}. \tag{77}$$

In Eqs. (76) and (77), the absorption coefficient due to diffuse scattering from defects in the jth layer is described by the following expression:

$$\mu^j_{\rm ds}(k_{0j}) = c_j C^2 {E_j}^2 m_{0j} J^j(k_{0j}),$$
$$m_{0j} = \frac{\pi v_{\rm c}}{4}(H_j|\chi_{{\rm r}\mathbf{H}_j}|/\lambda)^2, \tag{78}$$

$$J^j(k_{0j}) = \frac{1}{\pi {H_j}^2}\int {\rm d}\mathbf{k}' F_j(\mathbf{q}), \tag{79}$$

$$p'_j(d_j) = \frac{1-\exp(-2\mu_j d_j)}{2\mu_j d_j}. \tag{80}$$

As a rule, the angular width of diffuse scattering intensity distribution $\sim k_{\rm m}/K$ is significantly larger as compared with the width of the total reflection range, $W = 2|\chi_{\rm r\mathbf{H}}|[\sqrt{b}\sin(2\theta_{\rm B})]^{-1}$, where the influence of dynamical effects in diffuse scattering is substantial. Therefore, when integrating in Eq. (79), the dependence of the interference absorption coefficient $\mu_{\rm i}$ on exit angles $\Delta\theta'$ can be neglected because its influence is smoothed due to integration, and the quantity $\mu_{\rm i}$ in Eq. (67) can be replaced by its limiting value in the jth layer at $|\Delta\theta'| \gg W$:

$$\mu_j(\Delta\theta) = \frac{\mu_{0j}}{2\gamma_0}\frac{b+1}{2}\left[E_j\frac{r_{\rm i}(\Delta\theta)}{|g_j|}+1\right]. \tag{81}$$

Then the equalities $\mathbf{q} = \mathbf{k}_{0j} + \mathbf{k}' + i\mu_j\mathbf{n}$ and $|\mathbf{q}|^2 = k^2_{0j} + k'^2 + \mu^2_j$ hold, with the shortest distance from the reciprocal lattice point $\mathbf{H}_j$ to the Ewald sphere given by $k_{0j} = K(\Delta\theta + \Delta\theta_j)\sin(2\theta_{\rm B})$, and the integration in Eq. (79) can easily be performed:

$$J^j(k_{0j}) = \begin{cases} J^j_{\rm H}(k_{0j}) + J^j_{\rm H-SW}(k_{0j}), & \text{at} \quad |\mathbf{k}_{0j}| \leqslant k_{{\rm m}j} \\ J^j_{\rm SW}(k_{0j}), & \text{at} \quad |\mathbf{k}_{0j}| \geqslant k_{{\rm m}j} \end{cases}, \tag{82}$$

where the angular dependencies of the integral diffuse scattering intensity in one-dimensional Huang and Stokes-Wilson scattering regions ($|\mathbf{k}_{0j}| \leqslant k_{{\rm m}j}$ and $|\mathbf{k}_{0j}| \geqslant k_{{\rm m}j}$, respectively) are described as follows:

$$J^j_{\rm H}(k_{0j}) = b_2 \ln\frac{k^2_{{\rm m}j}+\mu^2_j}{k^2_{0j}+\mu^2_j} + \left(b_3 k^2_{0j} + b_4\mu^2_j\right) \times\left(\frac{1}{k^2_{{\rm m}j}+\mu^2_j} - \frac{1}{k^2_{0j}+\mu^2_j}\right), \tag{83}$$

$$J^j_{H-SW}(k_{0j}) = b_2 - \frac{1}{2}\frac{b_3 k^2_{0j} + b_4 {\mu_j}^2}{k^2_{mj}+{\mu_j}^2}, \tag{84}$$

$$J^j_{SW}(k_{0j}) = \frac{k^2_{mj}+{\mu_j}^2}{k^2_{0j}+{\mu_j}^2}\left(b_2 - \frac{1}{2}\frac{b_3 k^2_{0j} + b_4{\mu_j}^2}{k^2_{0j}+{\mu_j}^2}\right). \tag{85}$$

The coefficients b_i as well as the parameters $k_{{\rm m}j}$ and μ_j in Eqs. (83)–(85) are connected with defect characteristics via the following relationships:

$$b_2 = B_1 + \tfrac{1}{2}B_2\cos^2\theta_{\rm B}, \quad b_3 = B_2\left(\tfrac{1}{2}\cos^2\theta_{\rm B} - \sin^2\theta_{\rm B}\right),$$
$$b_4 = B_2\left(\tfrac{1}{2}\cos^2\theta_{\rm B} - \cos^2\psi\right), \tag{86}$$

where coefficients B_1 and B_2 for two types of defects are given in Eqs. (71) and (72).

It should be remarked that the absorption coefficients due to diffuse scattering in Eq. (77) above are the sums of corresponding coefficients in the case of several defect types randomly distributed in each layer. A similar superposition law is supposed to be valid for the exponent of the static Krivoglaz-Debye-Waller factor as well. The last one is also immediately connected with defect characteristics by the following relationships for dislocation loops and spherical clusters, respectively [69,78]:

$$L_{\mathbf{H}} \cong \tfrac{1}{2}n_{\rm L}R^3_{\rm L}(Hb)^{3/2}, \tag{87}$$

$$L_{\mathbf{H}} \cong \begin{cases} 0.525\, n_C v_C n_0 \eta^4, & \text{at} \quad \eta \leqslant 1.9 \\ n_C v_C n_0 \eta^3, & \text{at} \quad \eta > 1.9 \end{cases},$$
$$\eta = \sqrt{\Gamma|\varepsilon|H{\rm R}_C}, \quad n_0 = 4\pi {R_C}^3/(3v_{\rm c}), \tag{88}$$

where $n_L = c_L/v_{\rm c}$ and $n_C = c_C/v_{\rm c}$ are number densities of dislocation loops and spherical clusters (c_L and c_C are their concentrations); R_L and R_C are their radii, respectively.

The above-obtained formulas establish analytical relations between coherent and integral diffuse components of the reflection coefficients measured by high-resolution double-crystal diffractometers from imperfect multilayer structures in Bragg diffraction geometry, on the one hand, and statistical characteristics of defects in each layer, on the other hand. Of course, for full consistency these relations should be completed by known expressions for the additional average strain caused by randomly distributed defects of various types. In particular, the additional linear strain caused by circular prismatic dislocation loops and spherical clusters, respectively, is described by simple expressions [69]:

$$\varepsilon_{\rm L} = \frac{\pi}{3}|\mathbf{b}|R^2_{\rm L}n_{\rm L}, \quad \varepsilon_{\rm C} = \Gamma\varepsilon R^3_{\rm C}n_{\rm C}, \quad \varepsilon \approx \frac{1}{3}\frac{\Delta v_c}{v_c}. \tag{89}$$

Thus, the closed set of the analytical relationships is completed, which can provide the dynamical description of mutually consistent coherent and diffuse components of rocking curves measured by the high-resolution double-crystal x-ray diffractometer from imperfect multilayer systems. In consequence, it becomes possible to determine reliably both structural parameters of multilayers and characteristics of their defects by using the obtained formulas for the quantitative analysis of the rocking curves.

C. Diffuse scattering intensity integrated over vertical divergence

When the differential two-dimensional x-ray diffraction intensity distributions, i.e., reciprocal space maps, are measured by the triple-crystal diffractometer, the diffracted x-ray intensity is integrated only over vertical divergence. The corresponding diffuse component of the measured reflection

coefficient of the imperfect multilayer system can be determined then as follows:

$$r_{\rm diff}(\boldsymbol{\kappa}) = \int d\varphi R_{\rm DS}(\mathbf{k}), \tag{90}$$

where $\mathbf{k} = \boldsymbol{\kappa} + k_y\mathbf{e}_y$; the vector $\boldsymbol{\kappa} = k_x\mathbf{e}_x + k_z\mathbf{e}_z$ lies in the coherent scattering plane $(\mathbf{K}, \mathbf{H})$; the unit vectors $\mathbf{e}_y$ and $\mathbf{e}_z \equiv \mathbf{n}$ are directed perpendicularly to this plane and crystal surface, respectively; the unit vectors $\mathbf{e}_x$ and $\mathbf{e}_y$ lie in the crystal surface; and $k_y = K\varphi$.

After substituting Eq. (67) into Eq. (90) and carrying out the integration, we obtain the diffuse component of the differential x-ray diffraction intensity distribution from an imperfect multilayer system in the scattering plane, i.e., the diffuse component of the measured reciprocal space map:

$$r_{\rm diff}(\boldsymbol{\kappa}) = \sum_{j=0}^{M} F_j^{\rm ext} F_j^{\rm abs} r_{\rm diff}^{j}(\boldsymbol{\kappa}_j), \tag{91}$$

where the diffuse reflection coefficient of the jth layer in the two-dimensional Huang scattering region ($\kappa_j \leqslant k_{{\rm m}j}$) is given by the expression

$$r_{\rm diff}^{j}(\boldsymbol{\kappa}_j) = M_j[A_{\rm H}(\boldsymbol{\kappa}_j) + A_{\rm H,S-W}(\boldsymbol{\kappa}_j)],$$
$$M_j = c_j m_{0\,j} C^2 E_j^2 p(d_j)\frac{K d_j}{\pi\gamma_0} \tag{92}$$

In Eqs. (91) and (92), the vector $\boldsymbol{\kappa}_j = \boldsymbol{\kappa} + \Delta\mathbf{H}_j$ describes the deviation of the wave vector $\mathbf{K}'_j$ of a diffusely scattered wave from the reciprocal lattice point $\mathbf{H}_j$ in the jth layer, where $\Delta\mathbf{H}_j = \mathbf{H}_j - \mathbf{H}_0$ is the deviation from the reciprocal lattice vector $\mathbf{H}_0$ of the substrate, $\mathbf{H}_0^0\boldsymbol{\kappa}{=}k_x\sin\psi + k_z\cos\psi$, and $\mathbf{H}_j^0 = \mathbf{H}_j/H_j$ is a unit vector; $k_{{\rm m}j}$ and above mentioned vectors are presented in Fig. 3.

The terms $A_{\rm H}(\boldsymbol{\kappa}_j)$ and $A_{\rm H,S-W}(\boldsymbol{\kappa}_j)$ in Eq. (92) describe contributions from diffuse scattering intensity in Huang and Stokes-Wilson scattering regions after the integration over vertical divergence, respectively:

$$A_{\rm H}(\boldsymbol{\kappa}_j) = \frac{2B_{1\,j} + B_{2\,j}a(\boldsymbol{\kappa}_j)}{\sqrt{\kappa_j^2 + \mu_{i\,j}^2}}\arctan\frac{\sqrt{k_{m\,j}^2 - \kappa_j^2}}{\sqrt{\kappa_j^2 + \mu_{i\,j}^2}} + B_{2\,j}a(\boldsymbol{\kappa}_j)\frac{\sqrt{k_{mj}^2 - \kappa_j{}^2}}{\kappa_j{}^2 + \mu_{\rm ij}{}^2},$$
$$A_{\rm H,S-W}(\boldsymbol{\kappa}_j) = \frac{B_{1\,j} + \frac{3}{4}B_{2\,j}a(\boldsymbol{\kappa}_j)}{\sqrt{\kappa_j^2 + \mu_{i\,j}^2}}\left[\left(\frac{\pi}{2} - \arctan\frac{\sqrt{k_{m\,j}^2 - \kappa_j^2}}{\sqrt{\kappa_j^2 + \mu_{i\,j}^2}}\right)\frac{k_{m\,j}^2 + \mu_{i\,j}^2}{\kappa_j^2 + \mu_{i\,j}^2} - \frac{\sqrt{k_{m\,j}^2 - \kappa_j^2}}{\sqrt{\kappa_j^2 + \mu_{i\,j}^2}}\right] - \frac{1}{2}B_{2\,j}a(\boldsymbol{\kappa}_j)\frac{\sqrt{k_{m\,j}^2 - \kappa_j^2}}{\kappa_j^2 + \mu_{i\,j}^2},$$
$$a(\boldsymbol{\kappa}_j) = \frac{\left(\mathbf{H}_j^0\boldsymbol{\kappa}_j\right)^2 + \mu_{i\,j}^2\left(\mathbf{H}_j^0\mathbf{n}\right)^2}{\kappa_m{}^2 + \mu_{i\,j}^2}, \tag{93}$$

Similarly, for the diffuse reflection coefficient of the jth layer in the two-dimensional Stokes-Wilson scattering region ($\kappa_j \geqslant k_{{\rm m}\,j}$) one can obtain

$$r_{\rm diff}^{j}(\boldsymbol{\kappa}_j) = M_j A_{\rm S-W}(\boldsymbol{\kappa}_j), \tag{94}$$

$$A_{\rm S-W}(\boldsymbol{\kappa}_j) = \frac{\pi}{2}\left[B_{1\,j} + \frac{3}{4}B_{2\,j}a(\boldsymbol{\kappa}_j)\right]\frac{k_{m\,j}^2 + \mu_{i\,j}^2}{\left(\kappa_j^2 + \mu_{i\,j}^2\right)^{3/2}}. \tag{95}$$

Note that components k_x and k_z of the vector $\boldsymbol{\kappa}$ are connected with angular deviations of the investigated (ω) and analyzer (η) crystals from their exact reflecting positions by simple linear relationships. In the case of an asymmetric Bragg diffraction geometry, these relationships have the following form:

$$k_x = -K[\eta\sin(\theta_{\rm B} + \psi) - 2\omega\sin\theta_{\rm B}\cos\psi],$$
$$k_z = -K[\eta\cos(\theta_{\rm B} + \psi) + 2\omega\sin\theta_{\rm B}\sin\psi].$$

Thus, the analytical formulas obtained above in this subsection establish direct explicit relationships between the diffuse components of reciprocal space maps measured by the high-resolution triple-crystal diffractometer from imperfect multilayer structures in Bragg diffraction geometry, on the one hand, and strain, chemical composition, and statistical characteristics of defects in each layer, on the other hand. In combination with the derived analytical formulas for the coherent amplitude reflection coefficient they form the base for the dynamical description of mutually consistent coherent and diffuse scattering and quantitative analysis of measured reciprocal space maps for the sake of the reliable structural characterization of investigated imperfect multilayer systems.

V. DISCUSSION

A. Simulation of the rocking curve for InGaAs/GaAs superlattice with defects

The formulas obtained above in Secs. III B and IV B were used to simulate the rocking curve for the imperfect superlattice with defects, which consists of five periods of two layers, including 8 monolayers (ML) of $In_xGa_{1-x}As$ with In concentration $x = 0.4$ (Fig. 4) or $x = 0.2$ (Fig. 5), and 60 ML of GaAs, respectively, and was grown on a GaAs substrate. The simulated rocking curves have been calculated for the symmetrical (004) reflection of characteristic Cu Kα_1 radiation accounting for the convolution with an instrumental function of a typical high-resolution x-ray double-crystal diffractometer (DCD) [70].

Several types of structure imperfections have been chosen to demonstrate their influence on the high-resolution rocking curves measured from the imperfect superlattice. First of all, thermal atom vibrations are inevitably present at room temperature [Fig. 4(a)]. In addition, Fig. 4(b) shows the

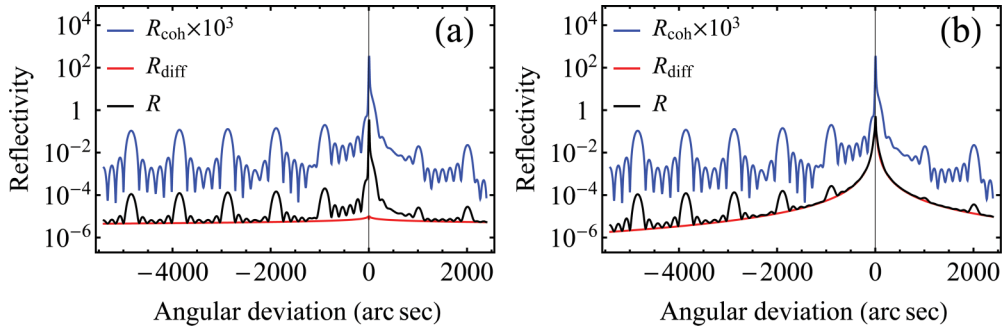

FIG. 4. Simulated rocking curves (R) and their coherent (R_{coh}) and diffuse (R_{diff}) components for the (004) reflection of Cu Kα_1 radiation from the imperfect InGaAs/GaAs superlattice containing structural defects of various types: thermal atom vibrations (a) and dislocation loops in GaAs substrate (b).

influence of dislocation loops randomly distributed in the GaAs substrate. Further, the changes in the rocking curve due to diffuse scattering from the disk-shaped inclusions of InAs particles (disk thickness $t_P = 1$ nm), which can be present in the $In_{0.4}Ga_{0.6}As$ layers of imperfect superlattice, were analyzed (Fig. 5). Characteristics of defects, including radius R, number density n, and strain at the cluster boundary ε, as well as corresponding diffraction parameters, namely, the exponent $L_{\mathbf{H}}$ of static Krivoglaz-Debye-Waller factor $E = \exp(-L_{\mathbf{H}})$, and maximal value of normalized absorption coefficient due to diffuse scattering in the jth layer under consideration, $m_j = \mu_{ds}(\Delta\theta_j)/\mu_0$, are given in Table I.

As can be seen in Fig. 4(a), where the calculated rocking curve (R) as well as its coherent (R_{coh}) and diffuse (R_{diff}) components are shown for the perfect $In_{0.4}Ga_{0.6}As$ superlattice on the perfect GaAs substrate, the contribution of thermal diffuse scattering intensity is distributed almost uniformly over a full angular range. Its magnitude is relatively small and becomes distinguishable, as compared with the coherent component, only on the far tails of the rocking curve.

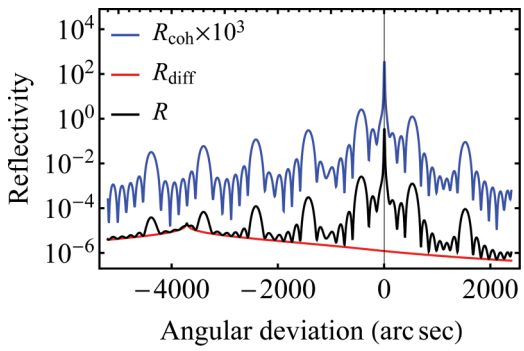

FIG. 5. Simulated rocking curve (R) and its coherent (R_{coh}) and diffuse (R_{diff}) components for the imperfect $In_{0.2}Ga_{0.8}As$ superlattice containing disk-shaped InAs particles (see Table I); symmetric GaAs (004) reflection, and Cu Kα_1 radiation. The peak of the diffuse component of multilayers is located at the Bragg angle, which corresponds to the structure of $In_{0.2}Ga_{0.8}As$ layers, and disposed between two satellites on the coherent component; mainly the right decreasing tail of the diffuse scattering intensity distribution can be seen in the considered angular range.

It should be noted that this picture would not be substantially changed when the optical branch of phonon dispersion relations is included into the consideration, since the contribution of optical phonons to the thermal Debye-Waller factor does not exceed several percent [77].

It is worthwhile to note also that the contribution to the total rocking curve due to the diffuse scattering from point defects, both in the substrate and superlattice layers, should be expected, in general, even smaller as compared with the contribution of thermal diffuse scattering intensity at room temperature.

Vice versa, the contribution of the diffuse scattering intensity from dislocation loops of submicrometer sizes in GaAs substrate is concentrated mainly under the substrate peak. Namely, its magnitude, as it was calculated for the circular prismatic dislocation loops randomly distributed in the GaAs substrate, with Burgers vector $\mathbf{b} = 1/2\langle 110\rangle$, is substantial at both substrate peak and nearest superlattice satellites and is remarkable even at far satellites [see Fig. 4(b)].

However, the most remarkable changes in the rocking curve shape features are caused by the inclusions of InAs particles in the layers of $In_{0.2}Ga_{0.8}As$ solid solution (Fig. 5). When choosing the characteristics of the disk-shaped InAs inclusions in the simulation, we took into account the necessity to fulfill the requirements of the present dynamical diffraction theory [66]. Namely, to satisfy the possibility of representing the crystal polarizability as the sum of average and fluctuating parts, the exponent of the static Krivoglaz-Debye-Waller factor must be sufficiently small; i.e.,

$$L_{\mathbf{H}} \ll 1. \tag{96}$$

In addition, to satisfy the superposition principle for the static displacement fields from the bounded defects, the average distance between defects r_0 must be significantly larger than the defect radius R_0; i.e.,

$$r_0 = (c/v_c)^{-1/3} \gg R_0. \tag{97}$$

In the present simulation, these parameters were chosen equal to $L_{\mathbf{H}} \approx 0.108$, $r_0 = 5$nm, and $R_0 = 79$ nm, respectively.

It should be noted here that the restrictions (96) and (97) are well satisfied for the case of dislocation loops in the GaAs substrate considered above as well; see Table I. However, the inequality (97) evidently does not hold in the case of the

TABLE I. Characteristics of defects in the imperfect $In_{0.4}Ga_{0.6}As$ (No. 1 and 2) and $In_{0.2}Ga_{0.8}As$ (No. 3) superlattice structures: radius (R), number density (n), and strain at the cluster boundary (ε), as well as corresponding diffraction parameters: exponent of static Krivoglaz-Debye-Waller factor ($L_{\mathbf{H}}$) and normalized coefficient of absorption due to diffuse scattering [$m_j = \mu^j_{\mathrm{ds}}(0)/\mu_0$].

No.	Type of defects	R (nm)	n (cm^{-3})	ε	$L_{\mathbf{H}}$	m_j
1	Thermal Ga atom vibrations	0.143	2.2×10^{22}	0.064	0.028	2.0×10^{-5}
	Thermal As atom vibrations	0.145	2.2×10^{22}	0.059	0.024	1.8×10^{-5}
2	Dislocation loops in GaAs substrate	300	5×10^{10}		0.051	2.0
3	InAs particles in $In_{0.2}Ga_{0.8}As$ layers	5	2×10^{15}	0.056	0.108	0.082

cluster model for the thermal diffuse scattering described in Sec. IV A. Just for this reason, to obtain reliable analytical estimations of the corresponding intensity distribution, the radii of effective clusters in this model were varied to provide the equality between the calculated static Krivoglaz-Debye-Waller factor and the known thermal Debye-Waller factor.

It should be emphasized that in the simulation procedure we took into account the mass conservation law for indium atoms; i.e., the InAs inclusions were supposed to be formed at the cost of indium atoms in the $In_{0.2}Ga_{0.8}As$ layers. Thus, the thickness of imperfect $In_{0.2}Ga_{0.8}As$ layers with InAs inclusions remains unchanged as compared with perfect ones. At the same time, the loss of indium atoms from $In_{0.2}Ga_{0.8}As$ matrix at the chosen parameters of InAs precipitates was so small that the change of the Bragg angle for these layers was only about 0.2 arc sec. As a consequence, the fine oscillation structure of the coherent component of the simulated rocking curve, which is only slightly distorted due to the small value of exponent of the static Krivoglaz-Debye-Waller factor, does not change remarkably as compared with the rocking curve of the perfect superlattice.

In turn, the immediate contribution of diffuse component to the total rocking curve of the imperfect $In_{0.2}Ga_{0.8}As$ superlattice remarkably affects the shape of the rocking curve as can be seen in Fig. 5. The maximum of diffuse scattering intensity from $In_{0.2}Ga_{0.8}As$ layers is located between two satellites at the Bragg angle corresponding to the $In_{0.2}Ga_{0.8}As$ layers, i.e., nearly at the angular deviation from the substrate peak $\Delta\theta \approx -3700$ arc sec. Therefore, we see mainly the right tail of the symmetric diffuse scattering intensity distribution in the angular range considered, which can be visually perceived as the asymmetric one.

It should be noted finally that the influence of the coefficient of absorption due to diffuse scattering on the attenuation of the coherent waves is negligibly small for the thermal diffuse scattering and relatively small for diffuse scattering from InAs inclusions in the InGaAs layers (see Table I). Only for dislocation loops in the GaAs substrate, the coefficient of absorption due to diffuse scattering in the close vicinity of substrate peak takes a value comparable with the coefficient of photoelectric absorption (cf. parameters m_j in Table I).

B. Simulation of the reciprocal space map for ion-implanted garnet film

The formulas obtained above in Secs. III B and IV C were used also to simulate the reciprocal space map for the epitaxial single-crystal yttrium iron garnet (YIG) film grown on a gadolinium gallium garnet (GGG) substrate and implanted with F^+ ions. The corresponding strain profile created in YIG film due to implantation with 90-keV F^+ ions at dose $D = 6 \times 10^{13}$ cm^{-2} is shown in Fig. 6 (for details see Ref. [79]).

The strain profile in the implanted subsurface layer of ion-implanted YIG film was supposed to be formed due to strain fields from secondary radiation defects like small spherical amorphous clusters. This fluctuating strain field from randomly distributed clusters can be represented as the sum of smooth "in average" and random components, which are homogeneous in the plane parallel to the film surface and inhomogeneous along the surface normal.

The depth profile of the average component of normal strain can be calculated through the depth-dependent average concentration of clusters $n_{\mathrm{C}}(z)$:

$$\varepsilon_{\perp}(z) = 3\Gamma\varepsilon n_{\mathrm{C}}(z) R_{\mathrm{C}}^3,$$

where ε is the strain at the cluster boundary and R_{C} is the cluster radius. When calculations of the diffraction intensity were performed, the implanted layer was subdivided into virtual laminae with randomly distributed defects and constant average strain in each lamina (Fig. 6).

The depth profile of the so-called amorphization factor is described by the static Krivoglaz-Debye-Waller factor. Namely, the exponent of this factor is calculated according to Eq. (88) through characteristics of clusters in the implanted layer, and its dependence on depth is described by the distribution of cluster concentration.

In addition, the depth dependence of the attenuation of the coherent component of diffraction intensity from the implanted layer is described along similar lines. Namely, the

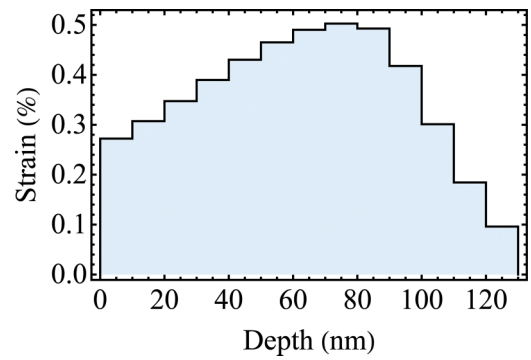

FIG. 6. Strain profile in the YIG film implanted with 90-keV F^+ ions at the dose $D = 6 \times 10^{13}$ cm^{-2}.

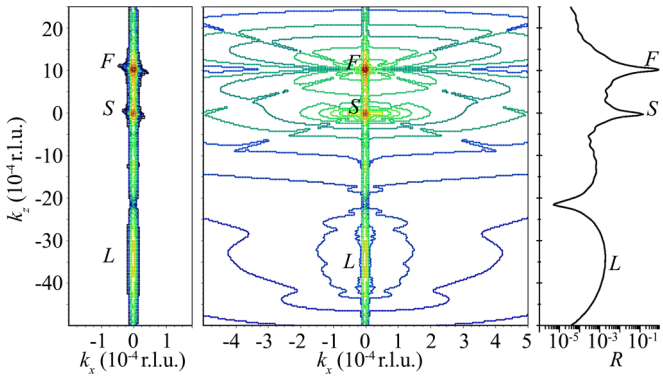

FIG. 7. Calculated reciprocal space map (in center), its coherent component (left), and longitudinal cross section (right) for 444 reflection of Cu Kα_1 radiation from YIG/GGG film system implanted with 90-keV F^+ ions at the dose $D = 6 \times 10^{13}$ cm^{-2}. Coherent peaks created from YIG film, GGG substrate, and ion-implanted layer are denoted by letters F, S, and L, respectively. Contours of equal intensity around these peaks are formed due to diffuse scattering from growth defects in the substrate and film, as well as owing to secondary radiation defects in the ion-implanted layer.

coefficient of absorption due to diffuse scattering is calculated through characteristics of clusters in the implanted layer by using Eqs. (78)–(86), where $c = n_C(z)/v_c$ should be put.

This diffraction model provides the physically clear connections between defect characteristics and diffraction parameters sensitive to crystal structure imperfections. The self-consistency between coherent and diffuse components of diffraction intensity is provided by such a model too.

As can be seen in Fig. 7, the diffuse scattering intensity distribution on the map is the superposition of three distributions. The first two are the regularly shaped diffuse scattering intensity distributions from microdefects, namely, randomly distributed clusters and dislocation loops of submicrometer sizes, in YIG film (of 5.33 μm thickness) and GGG substrate around corresponding reciprocal lattice points, respectively. The third is the irregularly shaped additional diffuse scattering intensity distribution caused by spherical amorphous clusters in the implanted YIG film layer (see defect characteristics in Table II).

It should be noted that the irregular shape of the diffuse scattering intensity distribution from spherical clusters in the implanted layer is formed due to their inhomogeneous concentration distribution in this layer. This inhomogeneity causes corresponding one-dimensional inhomogeneous in-

TABLE II. Characteristics of dislocation loops and spherical clusters in GGG substrate and YIG film implanted with 90-keV F^+ ions.

Layers	R_C (nm)	n_C (cm^{-3})	R_L (nm)	n_L (cm^{-3})
GGG substrate	8	1.0×10^{14}	90	1.2×10^{12}
YIG film	10	1.0×10^{14}	5	1.0×10^{15}
Implanted layer	1.7	6.0×10^{19}		

average strain field (see Fig. 6) and leads to smoothing and deformation of the double-drop form known for equidistant lines of the diffuse scattering intensity distributions from spherical clusters.

Similar, to some extent, nonuniform distributions of the diffuse scattering intensity were observed on some experimental reciprocal space maps. For example, one can point out the maps measured from GGG crystals implanted with 100-keV He^+ ions [80] or yttria-stabilized zirconia (YSZ) crystals irradiated with 4-MeV Au^{2+} ions [81]. The diffuse scattering intensity distributions observed in these investigations were significantly elongated as compared with that simulated above, which should be expected due to the smaller strain gradient at the significantly larger implantation depth.

VI. SUMMARY AND CONCLUSIONS

The generalized statistical dynamical theory of x-ray diffraction by the imperfect single crystals containing randomly distributed defects has been extended to characterize structural imperfections in real multilayers of arbitrary thickness as well as single crystals or crystalline films with inhomogeneous strain fields. The theoretical model developed for the case of Bragg diffraction geometry takes into account the presence of randomly distributed point defects and microdefects of various types as well as the existence of arbitrary inhomogeneous strain fields, in particular, with sharp profiles, i.e., with large strain gradients.

The proposed analytical derivation of the recurrence relations for coherent amplitude reflection and transmission coefficients of such multilayer systems, which consist of any number of real or virtual layers with nearly constant strains and randomly distributed defects, is based on the Ewald-Bethe-Laue consideration of the dynamical wave field in crystal structures with rigorous accounting for boundary conditions at layer interfaces. These relations and the analytical expressions obtained for diffuse components of reflection coefficients are immediately connected with statistical characteristics of defects in each layer due to using the Krivoglaz method of fluctuating waves of defect concentration.

Thus, the possibility is provided for the physically sound self-consistent dynamical description of coherent and diffuse components of the rocking curves and reciprocal space maps, which are measured by the high-resolution double- and triple-crystal diffractometers from imperfect multilayer crystal structures, respectively. As a consequence, the way is opened to significantly increasing the physical value of quantitative characterization results, which are obtained for structural imperfections in imperfect multilayers and single-crystalline structures with inhomogeneous strain fields by using the most informative and sensitive x-ray diffraction techniques.

ACKNOWLEDGMENTS

This research was supported by the National Academy of Sciences of Ukraine under Budget Program No. 6541230-3A and Contract No. III-12-18.

[1] V. Holý, U. Pietsch, and T. Baumbach, *High-Resolution X-Ray Scattering from Thin Films and Multilayers* (Springer, Berlin, Heideiberg, 1998).

[2] P. F. Fewster, *X-Ray Scattering from Semiconductors* (Imperial College Press, London, 2000).

[3] *Diffuse Scattering and the Fundamental Properties of Materials*, edited by R. I. Barabash, G. E. Ice, and P. E. A. Turchi (Momentum Press, New York, 2009).

[4] M. Schmidbauer, *X-Ray Diffuse Scattering from Self-Organized Mesoscopic Semiconductor Structures* (Springer, Berlin, Heidelberg, 2010).

[5] A. Benediktovich, I. Feranchuk, and A. Ulyanenkov, *Theoretical Concepts of X-Ray Nanoscale Analysis: Theory and Applications* (Springer Science & Business Media, Berlin, 2013).

[6] M. M. Karow, N. N. Faleev, D. J. Smith, and C. B. Honsberg, J. Cryst. Growth **425**, 43 (2015).

[7] C. Bergmann, A. Gröschel, J. Will, and A. Magerl, J. Appl. Phys. **118**, 015707 (2015).

[8] D. Tang, Y. Kim, N. Faleev, C. B. Honsberg, and D. J. Smith, J. Appl. Phys. **118**, 094303 (2015).

[9] A. V. Kuchuk, H. V. Stanchu, Ch. Li, M. E. Ware, Yu. I. Mazur, V. P. Kladko, A. E. Belyaev, and G. J. Salamo, J. Appl. Phys. **116**, 224302 (2014).

[10] N. Faleev, N. Sustersic, N. Bhargava, J. Kolodzey, A. Yu. Kazimirov, and C. Honsberg, J. Cryst. Growth **365**, 44 (2013).

[11] V. P. Kladko, A. V. Kuchuk, P. M. Lytvyn, O. M. Yefanov, N. V. Safriuk, A. E. Belyaev, Yu. I. Mazur, E. A. DeCuir, Jr., M. E. Ware, and G. J. Salamo, Nanoscale Res. Lett. **7**, 289 (2012).

[12] A. A. Minkevich, E. Fohtung, T. Slobodskyy, M. Riotte, D. Grigoriev, M. Schmidbauer, A. C. Irvine, V. Novák, V. Holý, and T. Baumbach, Phys. Rev. B **84**, 054113 (2011).

[13] M.-I. Richard, A. Malachias, J.-L. Rouvière, T.-S. Yoon, E. Holmström, Y.-H. Xie, V. Favre-Nicolin, V. Holý, K. Nordlund, G. Renaud, and T.-H. Metzger, Phys. Rev. B **84**, 075314 (2011).

[14] V. Kohli, M. J. Bedzyk, and P. Fenter, Phys. Rev. B **81**, 054112 (2010).

[15] V. Holý, J. Stangl, T. Fromherz, R. T. Lechner, E. Wintersberger, G. Bauer, C. Dais, E. Müller, and D. Grützmacher, Phys. Rev. B **79**, 035324 (2009).

[16] O. Kolomys, B. Tsykaniuk, V. Strelchuk, A. Naumov, V. Kladko, Yu. I. Mazur, M. E. Ware, S. Li, A. Kuchuk, Yu. Maidaniuk, M. Benamara, A. Belyaev, and G. J. Salamoless, J. Appl. Phys. **122**, 155302 (2017).

[17] A. Lomov, K. Shcherbachev, Y. Chesnokov, and D. Kiselev, J. Appl. Crystallogr. **50**, 539 (2017).

[18] I. Lobach, A. Benediktovitch, and A. Ulyanenkov, J. Appl. Crystallogr. **50**, 681 (2017).

[19] H. Kim, N. S. Bingham, A. Charipar, and A. Piqué, AIP Adv. **7**, 105116 (2017).

[20] V. S. Speriosu, J. Appl. Phys. **52**, 6094 (1981).

[21] V. S. Speriosu and T. Vreeland, J. Appl. Phys. **56**, 1591 (1984).

[22] E. E. Fullerton, I. K. Schuller, H. Vanderstraeten, and Y. Bruynseraede, Phys. Rev. B **45**, 9292 (1992).

[23] V. I. Punegov and Y. I. Nesterets, Pis'ma Zh. Tekh. Fiz. **20**, 62 (1994) [Sov. Tech. Phys. Lett. **20**, 64 (1994)].

[24] P. V. Petrashen, Fiz. Tverd. Tela **16**, 2168 (1974) [Solid State Phys. **17**, 2814 (1975)].

[25] A. M. Afanasev, M. V. Kovalchuk, E. K. Kovev, and V. G. Kohn, Phys. Status Solidi A **42**, 415 (1977).

[26] R. N. Kyutt, P. V. Petrashen, and L. M. Sorokin, Phys. Status Solidi A **60**, 381 (1980).

[27] V. G. Kohn, M. V. Kovalchuk, R. M. Imamov, and E. F. Lobanovich, Phys. Status Solidi A **64**, 435 (1981).

[28] L. Tapfer and K. Ploog, Phys. Rev. B **33**, 5565 (1986).

[29] V. Holý, J. Kuběna, E. Abramof, A. Pesek, and E. Koppensteiner, J. Phys. D: Appl. Phys. **26**, A146 (1993).

[30] F. N. Chukhovskii and Yu. P. Khapachev, Phys. Status Solidi A **88**, 69 (1985).

[31] N. Kato, Acta Crystallogr., Sect. A **48**, 834 (1992).

[32] Yu. N. Belyaev and A. V. Kolpakov, Phys. Status Solidi A **76**, 641 (1983).

[33] M. A. G. Halliwell, M. H. Lyons, and M. J. Hill, J. Cryst. Growth **68**, 523 (1984).

[34] D. M. Vardanyan, H. M. Manoukyan, and H. M. Petrosyan, Acta Crystallogr., Sect. A **41**, 212 (1985).

[35] M. A. Andreeva, K. Rosete, and Yu. P. Khapachev, Phys. Status Solidi A **88**, 455 (1985).

[36] W. J. Bartels, J. Hornstra, and D. J. Lobeek, Acta Crystallogr., Sect. A **42**, 539 (1986).

[37] C. R. Wie, T. A. Tombrello, and T. Vreeland, Jr., J. Appl. Phys. **59**, 3743 (1986).

[38] V. Holý, J. Kuběna, and K. Ploog, Phys. Status Solidi B **162**, 347 (1990).

[39] M. Dimer, E. Gerdau, R. Rüffer, H. D. Rüter, and W. Sturhahn, J. Appl. Phys. **79**, 9090 (1996).

[40] I. D. Feranchuk, S. I. Feranchuk, A. A. Minkevich, and A. Ulyanenkov, Phys. Rev. B **68**, 235307 (2003).

[41] L. De Caro and L. Tapfer, Phys. Rev. B **55**, 105 (1997); L. De Caro, C. Giannini, and L. Tapfer, *ibid.* **56**, 9744 (1997).

[42] S. A. Stepanov, E. A. Kondrashkina, R. Köhler, D. V. Novikov, G. Materlik, and S. M. Durbin, Phys. Rev. B **57**, 4829 (1998).

[43] A. Souvorov, T. Ishikawa, A. Y. Nikulin, Yu. P. Stetsko, S.-L. Chang, and P. Zaumseil, Phys. Rev. B **70**, 224109 (2004).

[44] T. A. Alexeeva, A. I. Benediktovich, I. D. Feranchuk, T. Baumbach, and A. Ulyanenkov, Phys. Rev. B **77**, 174114 (2008).

[45] A. Yu. Nikulin, A. W. Stevenson, and H. Hashizume, Phys. Rev. B **53**, 8277 (1996).

[46] A. Yu. Nikulin and P. V. Petrashen, J. Appl. Phys. **82**, 989 (1997).

[47] S. G. Podorov, G. Hölzer, E. Förster, and N. N. Faleev, Phys. Status Solidi A **169**, 9 (1998).

[48] U. Pietsch, V. Holý, and T. Baumbach, *High-Resolution X-Ray Scattering from Thin Films and Multilayers: From Thin Films to Lateral Nanostructures* (Springer, New York, 2004).

[49] N. N. Faleev, A. Yu. Egorov, A. E. Zhukov, A. R. Kovsh, S. S. Mikhrin, V. M. Ustinov, K. M. Pavlov, V. I. Punegov, M. Tabuchi, and Y. Takeda, Semiconductors **33**, 1229 (1999).

[50] A. Ulyanenkov, U. Klemradt, and U. Pietsch. Phys. B (Amsterdam, Neth.) **248**, 25 (1998).

[51] V. I. Punegov, Phys.-Usp. **58**, 419 (2015).

[52] P. V. Petrashen, Metallofizika **8**, 35 (1986); P. V. Petrashen, and F. N. Chukhovskii, *ibid.* **8**, 45 (1986).

[53] V. I. Punegov, Phys. Status Solidi A **136**, 9 (1993).

[54] K. M. Pavlov, V. I. Punegov, and N. N. Faleev, J. Exp. Theor. Phys. **80**, 1090 (1995).

[55] V. I. Punegov and N. N. Faleev, Fiz. Tverd. Tela **38**, 255 (1996).

[56] V. I. Punegov, K. M. Pavlov, S. G. Podorov, and N. N. Faleev, Fiz. Tverd. Tela **38**, 264 (1996).
[57] K. M. Pavlov and V. I. Punegov, Acta Crystallogr., Sect. A **54**, 214 (1998); **54**, 515 (1998).
[58] L. Kirste, K. M. Pavlov, S. T. Mudie, V. I. Punegov, and N. Herres, J. Appl. Crystallogr. **38**, 183 (2005); P. K. Shreeman and R. J. Matyi, *ibid.* **43**, 550 (2010); Phys. Status Solidi A **208**, 2533 (2011).
[59] V. I. Punegov and N. N. Faleev, JETP Lett. **92**, 437 (2010).
[60] N. N. Faleev, C. Honsberg, and V. I. Punegov, J. Appl. Phys. **113**, 163506 (2013).
[61] V. A. Bushuev, Sov. Phys. Solid State **31**, 1877 (1989); Sov. Phys. Crystallogr. **34**, 163 (1989).
[62] N. Kato, Acta Crystallogr., Sect. A **36**, 763 (1980); **36**, 770 (1980).
[63] V. Holý and K. T. Gabrielyan, Phys. Status Solidi B **140**, 39 (1987).
[64] A. M. Polyakov, F. N. Chukhovskii, and D. I. Piskunov, Sov. Phys. - JETP **72**, 330 (1991).
[65] N. Kato, Acta Crystallogr., Sect. A **47**, 1 (1991).
[66] V. B. Molodkin, S. I. Olikhovskii, E. N. Kislovskii, E. G. Len, and E. V. Pervak, Phys. Status Solidi B **227**, 429 (2001).
[67] S. I. Olikhovskii, V. B. Molodkin, E. N. Kislovskii, E. G. Len, and E. V. Pervak, Phys. Status Solidi B **231**, 199 (2002).
[68] M. von Laue, *Röntgenstrahlinterferenzen* (Akademische Verlagsgesellschaft, Leipzig, 1948).
[69] M. A. Krivoglaz, *Diffraction of X-Rays and Thermal Neutrons in Imperfect Crystals* (Springer, Berlin-Heidelberg, 1992).
[70] V. B. Molodkin, S. I. Olikhovskii, E. N. Kislovskii, T. P. Vladimirova, E. S. Skakunova, R. F. Seredenko, and B. V. Sheludchenko, Phys. Rev. B **78**, 224109 (2008).
[71] V. B. Molodkin, S. I. Olikhovskii, E. G. Len, E. N. Kislovskii, V. P. Kladko, O. V. Reshetnyk, T. P. Vladimirova, and B. V. Sheludchenko, Phys. Status Solidi A **206**, 1761 (2009).
[72] V. B. Molodkin, S. I. Olikhovskii, Ye. M. Kyslovskyy, I. M. Fodchuk, E. S. Skakunova, E. V. Pervak, and V. V. Molodkin, Phys. Status Solidi A **204**, 2606 (2007).
[73] R. N. Kyutt, A. Yu. Khilko, and N. S. Sokolov, Appl. Phys. Lett. **70**, 1563 (1997).
[74] P. H. Dederichs, Phys. Rev. B **4**, 1041 (1971); **1**, 1306 (1970).
[75] C. Kittel, *Introduction to Solid-State Physics* (John Wiley & Sons, Inc. New York, 1986).
[76] M. Schowalter, A. Rosenauer, J. T. Titantah, and D. Lamoen, Acta Crystallogr., Sect. A **65**, 5 (2009).
[77] J. F. Vetelino, S. P. Gaur, and S. S. Mitra, Phys. Rev. B **5**, 2360 (1972).
[78] O. S. Skakunova, Metallofiz. Noveishie Tekhnol. **37**, 555 (2015).
[79] O. S. Skakunova, V. M. Pylypiv, S. J. Olikhovskii, T. P. Vladimirova, B. K. Ostafiychuk, V. B. Molodkin, Ye. M. Kyslovs'kyy, O. V. Reshetnyk, O. Z. Garpul', A. V. Kravets, and V. L. Makovs'ka, Metallofiz. Noveishie Tekhnol. **34**, 1325 (2012).
[80] B. K. Ostafiychuk, I. P. Yaremiy, S. I. Yaremiy, V. D. Fedoriv, U. O. Tomyn, M. M. Umantsiv, I. M. Fodchuk, and V. P. Kladko, Crystallogr. Rep. **58**, 1017 (2013).
[81] A. Debelle, J. Channagiri, L. Thomé, B. Décamps, A. Boulle, S. Moll, F. Garrido, M. Behar, and J. Jagielski, J. Appl. Phys. **115**, 183504 (2014).